WILEY

RESEARCH ARTICLE

Addressing challenges of high spatial resolution UHF fMRI for group analysis of higher-order cognitive tasks: An inter-sensory task directing attention between visual and somatosensory domains

Kevin M. Aquino[1,2,3] | Rodika Sokoliuk[4] | Daisie O. Pakenham[1] | Rosa Maria Sanchez-Panchuelo[1] | Simon Hanslmayr[4] | Stephen D. Mayhew[4] | Karen J. Mullinger[1,4] | Susan T. Francis[1]

[1]Sir Peter Mansfield Imaging Centre, School of Physics and Astronomy, University of Nottingham, Nottingham, United Kingdom

[2]Brain and Mental Health Laboratory, Monash University, Clayton, Australia

[3]School of Physics, University of Sydney, Sydney, Australia

[4]Centre for Human Brain Health, School of Psychology, University of Birmingham, Birmingham, United Kingdom

Correspondence
Kevin M. Aquino, Brain and Mental health Laboratory, Monash Institute of Cognitive and Clinical Neurosciences, 770 Blackburn Rd, Clayton 3800, Victoria, Australia.
Email: kevin.aquino@monash.edu

Abstract

Functional MRI at ultra-high field (UHF, ≥7 T) provides significant increases in BOLD contrast-to-noise ratio (CNR) compared with conventional field strength (3 T), and has been exploited for reduced field-of-view, high spatial resolution mapping of primary sensory areas. Applying these high spatial resolution methods to investigate whole brain functional responses to higher-order cognitive tasks leads to a number of challenges, in particular how to perform robust group-level statistical analyses. This study addresses these challenges using an inter-sensory cognitive task which modulates top-down attention at graded levels between the visual and somatosensory domains. At the individual level, highly focal functional activation to the task and task difficulty (modulated by attention levels) were detectable due to the high CNR at UHF. However, to assess group level effects, both anatomical and functional variability must be considered during analysis. We demonstrate the importance of surface over volume normalisation and the requirement of no spatial smoothing when assessing highly focal activity. Using novel group analysis on anatomically parcellated brain regions, we show that in higher cognitive areas (parietal and dorsal-lateral-prefrontal cortex) fMRI responses to graded attention levels were modulated quadratically, whilst in visual cortex and VIP, responses were modulated linearly. These group fMRI responses were not seen clearly using conventional second-level GLM analyses, illustrating the limitations of a conventional approach when investigating such focal responses in higher cognitive regions which are more anatomically variable. The approaches demonstrated here complement other advanced analysis methods such as multivariate pattern analysis, allowing UHF to be fully exploited in cognitive neuroscience.

KEYWORDS

fMRI, 7 T, attention modulation, directed attention, MRI, multi-sensory domain, somatosensory, ultra-high field, visual

1 | INTRODUCTION

The development of ultra-high field (UHF, ≥ 7 T) MRI scanners has provided new opportunities for functional MRI (fMRI). Increasing the field strength results in the intrinsic increase in image signal-to-noise ratio (SNR) (Pohmann, Speck, & Scheffler, 2016; Vaughan et al., 2001) and this, coupled with an increased blood oxygenation level-dependent (BOLD) signal change, results in increased BOLD contrast-to-noise ratio (CNR). This can be exploited to improve the spatial resolution of fMRI data or to enhance the sensitivity, enabling the detection of weaker responses.

Karen J. Mullinger and Susan T. Francis contributed equally to this study.

To date, the majority of UHF fMRI studies have used reduced field-of-view (FOV) 2D-and 3D echo planar imaging (EPI) acquisitions to study chosen primary sensory areas, such as the visual and sensori-motor cortices (Fracasso, Luijten, Dumoulin, & Petridou, 2017; Puckett, Bollmann, Barth, & Cunnington, 2017; Reithler, Peters, & Goebel, 2017; Schluppeck, Sanchez-Panchuelo, & Francis, 2017), thus overcoming a number of challenges of B_0 and B_1 inhomogeneities associated with larger FOV acquisitions (Polimeni, Renvall, Zarets-kaya, & Fischl, 2017; Uludag & Blinder, 2017). For example, the increase in BOLD CNR of UHF experiments has been used to provide detailed maps of individual subjects' visual (Goncalves et al., 2015; Kemper, De Martino, Emmerling, Yacoub, & Goebel, 2017; Poltoratski, Ling, McCormack, & Tong, 2017; Rua et al., 2017) and somatosensory functional responses (Puckett et al., 2017; Sanchez Panchuelo et al., 2016; Sanchez Panchuelo, Schluppeck, Harmer, Bowtell, & Francis, 2015) and how these relate to individual brain anatomy (Besle, Sanchez-Panchuelo, Bowtell, Francis, & Schluppeck, 2014; Sanchez-Panchuelo et al., 2012; Sanchez-Panchuelo et al., 2014). These functional maps have been shown to spatially vary across subjects, highlighting inter-subject variability, whilst the reproducibility of these maps has been shown to be high within subjects across sessions (Goncalves et al., 2015; Sanchez-Panchuelo et al., 2012). Imaging at the sub-millimetre level has allowed mapping of cortical columns and 'layers' of cortex (e.g., De Martino et al., 2015; Kok, Bains, van Mourik, Norris, & de Lange, 2016; Muckli et al., 2015; Olman et al., 2012; Yacoub, Shmuel, Logothetis, & Ugurbil, 2007; Zimmermann et al., 2011), providing a novel method by which to distinguish bottom-up and top-down neural processes (Kok et al., 2016; Muckli et al., 2015; Olman et al., 2012).

The challenges of full FOV acquisitions at UHF have resulted in there being a limited number of studies of whole brain function at high spatial resolution to date (e.g., Boyacioglu et al., 2014; Goodman et al., 2017; Mestres-Misse, Trampel, Turner, & Kotz, 2017; Vu et al., 2016). In particular there are few studies of cognitive function, as highlighted in a recent review article (De Martino et al., 2017). Although full FOV functional acquisitions are now included in the Human Connectome Project 7 T protocol (http://protocols. humanconnectome.org/) for resting state assessment. However, large inter-individual differences in anatomy can arise (Geyer, Weiss, Reimann, Lohmann, & Turner, 2011; Gu & Kanai, 2014; Kanai & Rees, 2011) which results in challenges in the data analysis of group functional responses, meaning responses might be lost at the group level due to lack of spatial congruency. To date, to our knowledge, only three studies have used whole brain UHF fMRI to map responses to complex cognitive tasks in higher-order cortical regions (Goodman et al., 2017; Torrisi et al., 2018; Vu et al., 2016). Goodman et al. (2017) exploited 7 T to investigate the neural basis of consumer buying motivations. This study maximised the increased BOLD CNR of UHF, but did not realise the full potential of 7 T as a 6 mm full-width-at-half-maximum (FWHM) smoothing kernel was applied to GE-EPI data acquired at 2 mm isotropic to reveal the group activity. Vu et al. (2016) exploited the benefits of high 500 ms temporal reso-lution to show the improved sensitivity of capillary responses at 7 T compared with 3 T allowing the decoding of fine-grained temporal information for word classification. Torrisi et al. (2018) compared the benefits of using 7 T over 3 T fMRI in a go no-go task. This study had

a particular focus on increased statistical power at UHF, and showed that high power can be gained with fewer subjects, but as in Goodman et al., the 6 mm Gaussian smoothing applied meant the acquisition did not realise the full activation spatial resolution achievable at 7 T.

UHF provides the potential to study cognitive processing with high BOLD CNR to enable the detection of more subtle cognitive responses and/or the precise characterisation of responses on an indi-vidual subject level. However, it is expected that the spatial location of brain function in higher cortical regions may be more variable between subjects than in primary sensory cortex due to the combina-tion of inter-individual anatomical differences in brain structure and/or spatial differences in functional responses. Thus a method by which brain structure and function can be studied on an individual subject basis and linked to behaviour would be highly beneficial to the advancement of cognitive neuroscience.

Here, we investigate whole brain higher-order cognitive function to an adapted Posner paradigm, a classic paradigm in cognitive neuro-science, using high spatial resolution UHF (7 T) fMRI. This adapted Pos-ner, visual/somatosensory top-down attention modulation task is used to assess brain regions involved in varying the degree of attention directed to the somatosensory and visual domains. We explore the effect of inter-subject structural and functional differences in higher-order cortical regions, and assess the effect of normalisation and smoothing pre-processing steps on the resultant group functional maps. Typically, a Posner paradigm is used to modulate visual spatial attention (e.g., Corbetta, Kincade, Ollinger, McAvoy, & Shulman, 2000; Gitelman et al., 1999; Gould, Rushworth, & Nobre, 2011; Posner, 1980), but has been less commonly used to modulate spatial attention in the somatosensory domain (e.g., Haegens, Handel, & Jensen, 2011; Haegens, Luther, & Jensen, 2012; Wu et al., 2014). In electroencepha-lography (EEG), these attention modulations have been associated with increased hemispheric lateralisation of the power of alpha-frequency (8–13 Hz) oscillations over sensory-specific areas with increased spatial attention to a location (i.e., a contralateral decrease and ipsilateral increase in alpha power relative to the attention location) (Gould et al., 2011; Haegens et al., 2011; Haegens et al., 2012; Rihs, Michel, & Thut, 2007; Worden, Foxe, Wang, & Simpson, 2000; Zumer, Scheeringa, Schoffelen, Norris, & Jensen, 2014). This alpha modulation has been associated with a decrease in inhibition/increase in cortical excitability in the relevant cortical areas when attention is directed to its corre-sponding spatial location (Gould et al., 2011; Haegens et al., 2011; Hae-gens et al., 2012; Rihs et al., 2007; Worden et al., 2000; Zumer et al., 2014). In fMRI studies, Posner paradigms have been widely used to identify brain regions involved with visual spatial attention (Carrasco, 2011; Corbetta et al., 2000; Gitelman et al., 1999 ; Martinez et al., 1999), identifying modulations across a number of cortical regions including the frontal eye fields (FEF), posterior parietal, cingulate, stri-ate and extrastriate cortex (Gitelman et al., 1999; Martinez et al., 1999), with the intraparietal sulcus (IPS) recruited specifically during the cued attention period prior to stimulus presentation (Corbetta et al., 2000). Whilst tactile spatial attention has been studied less com-monly with EEG and fMRI, the inferior parietal lobule and secondary somatosensory cortex (SII) have been shown to be recruited (Gomez-Ramirez, Hysaj, & Niebur, 2016; Wu et al., 2014). To our knowledge, only one previous fMRI study has investigated the brain activity

underlying manipulation of spatial attention across two sensory modalities in a single task using a Posner-style paradigm (Macaluso, Eimer, Frith, & Driver, 2003). The authors showed that directing attention spatially to the right or left side of the visual domain or tactile (somatosensory) domain generated two forms of attentional brain response, termed 'unimodal' and 'multimodal'. Unimodal effects were found in regions where responses were only seen for attention to that specific modality; with the superior occipital and fusiform gyrus recruited by vision and the post-central gyrus by touch. Multimodal effects were independent of the attended sensory modality, and even observed when no stimulus was presented (only attention directed); these effects were strongest in superior premotor areas and the left inferior parietal lobule, but also seen in posterior parietal and prefrontal cortices. These previous studies illustrate that these paradigms recruit top-down attentional modulation and involve higher cortical frontal–parietal areas as well as primary sensory regions, thus providing an ideal paradigm for testing and developing the utility of UHF fMRI for cognitive studies. To our knowledge, the areas involved in both directing and modulating attention between sensory modalities, such that attention is divided between the modalities, are currently unknown and provide an excellent test of UHF fMRI in the identification of the higher-order cognitive areas, where only subtle differences in the amplitude of the BOLD response between conditions are expected.

In summary, the benefits and challenges of performing a group analysis of a large FOV, whole brain study of higher-order cognition at 7 T are presented. We aim to demonstrate the optimal analysis methods to study whole brain focal, higher-order cortical responses at the group level, where differences in BOLD response between conditions are subtle and individual anatomical and functional variability are evident. fMRI data are analysed on the cortical surface at both the individual subject and group level. At the group level, normalisation using both volume and surface registration is assessed, along with the dependency on spatial smoothing. We hypothesise that using optimised analysis methods we will observe: (1) linear modulations of BOLD signal by attention in primary sensory regions (akin to modulation of EEG alpha power with the direction of spatial attention; Gould et al., 2011); (2) sensory modality independent modulations of BOLD signal (i.e., only dependent on how attention is split between modalities) in higher-order cortical regions, such as parietal cortex and FEF (Macaluso et al., 2003).

2 | METHODS

2.1 | Subjects

This study was conducted with approval from the local ethics committee and complied with the Code of Ethics of the World Medical Association (Declaration of Helsinki). All subjects gave written informed consent. Data were acquired from 10 experienced fMRI subjects (age 28 ± 5 years [mean $\pm$ SD], 4 female).

2.2 | MRI acquisition procedures

All MR data were acquired on a 7 T Philips Achieva MR scanner (Philips Medical Systems, Best, Netherlands), with head-only transmit coil and 32-channel receive coil (Nova Medical, Wilmington). Foam padding was used to minimise head movement.

2.2.1 | Attention modulation scan session

To ensure whole brain coverage with high temporal and spatial resolution a multiband (MB) [or simultaneous multi-slice (SMS)] (GyroTools Ltd, Zurich, Switzerland) gradient echo echo-planar imaging (GE-EPI) sequence was employed (TR = 1.9 s, TE = 25 ms, 1.5 mm isotropic resolution, 128 $\times\times$ 131 matrix, multiband factor 2, 75° flip angle (FA), SENSE factor 2.5, receiver bandwidth 1,172 Hz/pix, phase encoding (PE) direction: anterior–posterior). 58 contiguous axial slices covering visual, somatosensory and attention-related regions (parietal cortex, dorsal-lateral prefrontal cortex [DLPFC]) were collected in the given TR period. B_0-field maps were acquired (TR = 26 ms, TE = 5.92 ms, ΔTE = 1 ms, 4 mm isotropic resolution, 64 × 64 matrix, 40 slices, FA =25°, SENSE factor 2) and local image-based (IB) shimming performed, thus limiting field perturbations in B_0 over the whole brain FOV in the fMRI acquisitions.

A total of 210 fMRI volumes were acquired per run, with 30 s/80 s of baseline data collected at the start/end of each run whilst subjects fixated on a dot. MB data were reconstructed offline (CRecon, GyroTools Ltd). During all fMRI scans, cardiac and respiratory traces were recorded for physiological correction due to the known increase in physiological to thermal noise ratio at 7 T (Triantafyllou et al., 2005; Triantafyllou, Hoge, & Wald, 2006). A peripheral pulse unit (PPU) on the subject's left ring finger was used to record the cardiac trace, and a pneumatic belt placed around the chest was used to record respiration.

In the same scan session, a high-resolution whole brain phase-sensitive inversion recovery (PSIR) sequence (Mougin et al., 2016) [0.7 mm isotropic resolution, 288 × 257 matrix, 98 slices, TI = 785/2,685 ms, SENSE factors: 2.2 (right–left, phase encode), 2 (foot-head, slice selection)] was also acquired for segmentation and cortical flattening.

2.2.2 | Retinotopic mapping scan session

To explore inter-subject differences in the structure of higher-order cortical regions as compared with primary visual areas, and its likely contribution to inter-subject differences in the spatial location of activation, a retinotopic mapping task was performed on all subjects. This provided functional boundaries in primary visual cortex, allowing comparison of functional and anatomically defined boundaries in a primary sensory region. Retinotopy GE-EPI fMRI data were acquired in a separate scan session (TR = 2 s, TE = 25 ms, 1.5 mm³ isotropic resolution, 124 × 121 matrix, 85° FA, SENSE factor 2.5, receiver bandwidth 1,089 Hz/pix, PE direction: foot-head). About 32 coronal oblique slices were acquired to cover the entire visual stream (V1 to IPS), with IB shimming performed over this target region, and 120 volumes collected per run.

2.3 | Paradigm

2.3.1 | Attention modulation paradigm

Subjects viewed a projector screen through prism glasses whilst lying supine in the scanner bore. A variant of the Posner paradigm (Posner,

1980) was used to modulate attention between visual [V] and somatosensory [S] domains, as shown in Figure 1a. This comprised of a 250 ms duration visual cue at the start of each trial to indicate the certainty (0, 40, 60, or 100%) of the target appearing in the visual domain (Figure 1a, cues panel). This was followed by a blank screen with a central white fixation dot, which was presented for an asynchronous inter-stimulus-interval (aISI) of variable length of 1.3–1.6 s prior to stimulus presentation. During this aISI subjects were instructed to allocate their attention between the visual and somatosensory domains, according to the cue certainty. A target stimulus (high or low frequency) was then presented in either the visual or somatosensory domain, with a distractor stimulus (middle frequency) presented concurrently in the other sensory domain. The visual stimuli comprised a Gabor grating presented for 66.7 ms with spatial frequency of 3.2 (low), 6.4 (middle) or 12.8 (high) degrees/cycle which filled a visual angle of 2.1° in the lower left visual field (at 5.2/2.6° of visual angle in the horizontal/vertical planes). The somatosensory stimuli were delivered at 4, 16 or 52 Hz for 250 ms to the tip of left index finger using a 7 T compatible piezoelectric stimulator (Dancer Design, St. Helens, United Kingdom, http://www.dancerdesign.co.uk). The different stimulus durations between the visual and somatosensory stimuli were required to ensure comparable task behaviour responses across sensory domains (validated prior to the fMRI study). Subjects were required to respond as quickly as possible after stimulus presentation, with a button press of the right index or middle finger to indicate if the target stimulus was delivered at low or high frequency, providing accuracy scores and reaction time measures. An 850 ms period was allowed for subjects to respond to the stimulus presentation before the visual cue for the next trial was presented.

Trials were presented in blocks to ensure high sensitivity to the attention modulation. About 25 trials of a given cue condition (S/V: 100/0, 60/40, 40/60, 0/100) were presented in a block before switching to a different attention condition. Within one fMRI run, blocks of each of the four attention conditions were presented in a pseudo random order. A total of four fMRI runs were acquired in a single scan session giving a total of 100 trials per condition over all runs (see schematic in Figure 1b). The stimulus paradigm was controlled by Psych-toolbox (ptb v3 – http://psychtoolbox.org/overview/). At the end of each fMRI run the subject was given visual feedback to inform them of their performance (accuracy of target classification). Approximately 10 min rest was allowed between runs with no fMRI acquisition, providing a break for subjects. The total time to collect the four runs was 27 min, disregarding the 10 min rest periods between runs.

Prior to entering the MR scanner, subjects performed one run of the fMRI paradigm (i.e., 25 trials of each condition) to minimise learning effects during the fMRI acquisition and ensure they could perform the task well.

2.3.2 | Retinotopic mapping paradigm

Eccentricity and polar angle maps were measured using standard retinotopic mapping procedures comprising an expanding annulus and rotating wedge to define visual areas (V1, V2, V3, V4) for each subject, akin to (Gardner, Merriam, Movshon, & Heeger, 2008). These are standard retinotopic stimuli provided in the mgl toolbox (version 2.0 https://github.com/justingardner/mgl). Eccentricity was measured using an expanding annulus that started from a fixation point at the fovea and moved out to the periphery to map visual eccentricity. To measure polar angle in visual cortex, a wedge rotated clockwise. Both the annulus and wedge stimuli
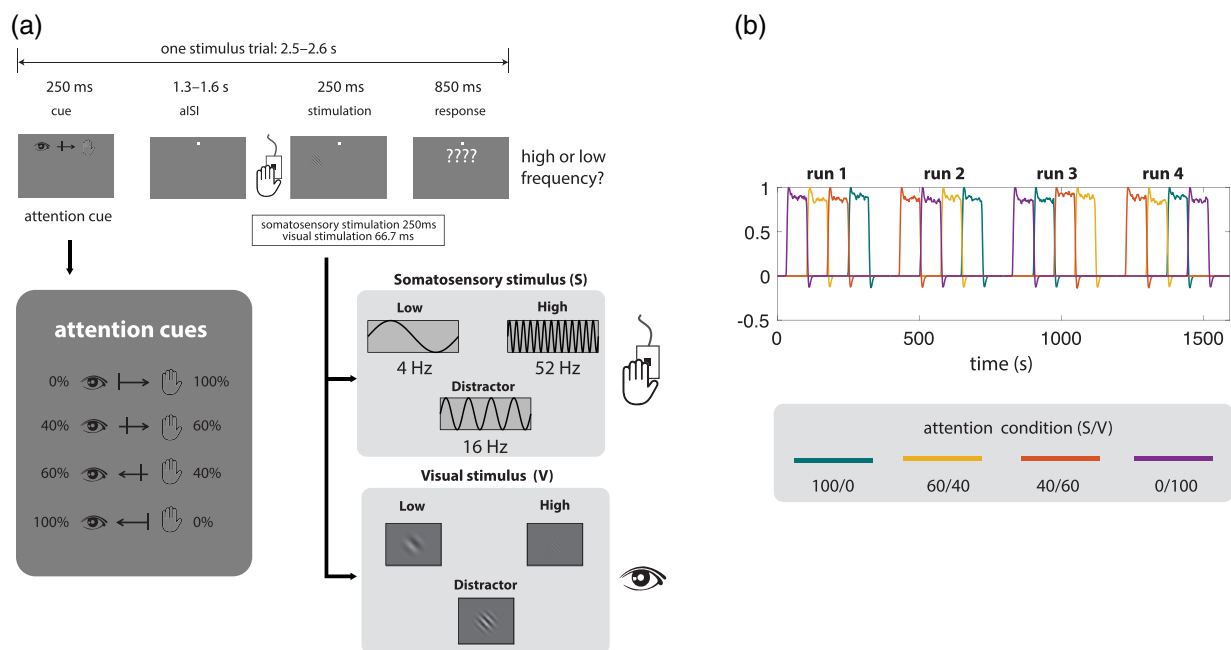

FIGURE 1 Schematic showing the attention paradigm. (a) Illustration of a single trial, inserts show all possible cue and stimulus presentations within a trial. The hand indicates which hand underwent the somatosensory stimulus, and the box is a schematic representation of the piezoelectric stimulator. (b) Schematic showing full fMRI experiment. Trials (a) were presented in blocks of 25 of the same cue condition (e.g., 100% V) before switching to another cue condition (e.g., 40% V, as shown in run 1). Cues were presented in a pseudo-random order across runs. A 10 min rest period (not shown) was provided between runs [Color figure can be viewed at wileyonlinelibrary.com]

were textured with a checkerboard with alternating chromatic contrast. One period of stimulation (i.e., a full expansion from fovea to the periphery or a complete clock-wise rotation of the wedge) took 24 s, with 10 repeats collected per scan. For both annuli and wedges, a second scan was collected with reverse order (i.e., from expansion to contraction, or clock-wise to counter-clockwise) to control for the spatiotemporal haemodynamic response function (Aquino, Schira, Robinson, Drysdale, & Breakspear, 2012). For all conditions subjects fixated on a central cross which flickered between red and grey.

3 | ANALYSIS

3.1 | Behaviour

To test the efficacy of the paradigm in modulating attention, three-way repeated measures ANOVAs were performed on the accuracy and reaction time measures acquired during the fMRI task. Data were tested for significant effects of cue (i.e., 0/100% compared with 40/60% attention), modality (i.e., attending to the somatosensory or visual modality) and subject (i.e., whether behaviour was the same for all subjects). When significant interactions were found, post-hoc analyses using paired t-tests were performed to identify the conditions driving the observed differences.

3.2 | MRI pre-processing

3.2.1 | Functional MRI data

fMRI data were first corrected for physiological noise to remove cardiac and respiratory associated noise using retrospective image correction (RETROICOR) (Glover, Li, & Ress, 2000). Images were motion corrected (SPM12, http://www.fil.ion.ucl.ac.uk/spm/software/spm12/) to the first GE-EPI volume within each fMRI run, and then between fMRI runs by registering all data to the mean GE-EPI image of the second fMRI run. The functional images were then corrected for scanner drift by regressing out a linear drift between the initial and final rest periods of each run.

3.2.2 | Anatomical MRI data

PSIR data were processed to derive a bias-field corrected PSIR image (Mougin et al., 2016) by polarity restoring (using the phase) the first inversion time (785 ms) and dividing by the sum of the modulus of the two inversion time images (785 and 2,685 ms). The PSIR images were then automatically segmented into grey and white matter using Freesurfer V6.0 [freesurfer.net], taking care to manually correct any segmentation errors. The two interfaces between grey/white matter and grey matter/cerebral spinal fluid (CSF) generated the *white* and *pial* surfaces, respectively.

The mean GE-EPI image across all runs of a paradigm (attention or retinotopy) was then used to co-register from fMRI data space to PSIR data space using a linear affine transform (mrTools, http://gru.stanford.edu/doku.php/mrtools/overview).

3.3 | Subject normalisation

Subjects' fMRI data were normalised into a standard space for group analyses. Both volume and surface based registration techniques were performed for comparison. These steps are summarised in Figure 2, with the processing pipelines described in detail below.

3.3.1 | Volume normalisation

For volume normalisation, subjects' PSIR data were registered to the Montreal Neuroimaging Institute (MNI) 152 space using a 'symmetric normalisation' algorithm employed in the advanced normalisation tools [ANTS http://stnava.github.io/ANTs/, (Avants et al., 2011; Avants, Tustison, & Song, 2009; Klein et al., 2009)]. This has been shown to provide a superior method for nonlinear registration, outperforming other volume-level normalisation such as SPM12's 'unified segmentation'. Warping parameters were then applied to the pre-processed fMRI data (see Figure 2, solid lines path).

3.3.2 | Surface normalisation

For surface normalisation, subjects' PSIR data were registered to a surface generated from MNI 305, Freesurfer's average subject template *fsaverage*, described in Fischl, Sereno, and Dale (1999). In brief, registration was performed in two steps. First, the PSIR segmentations were inflated and the vertices from the individual subject surface were mapped onto an individual subject spherical representation of the brain and curvature information regarding the folding patterns of the gyri and sulci for the individual subjects derived (standard procedure in Freesurfer). The individual subject folding patterns were then used to register these surfaces to the normalised *fsaverage* surface, which had been mapped onto a sphere, as previously described (Fischl, Sereno, Tootell, & Dale, 1999). Second, fMRI data were interpolated onto the individual subject cortical surface and a 'white' layer, pial layer and mid-layer (at 50% of the surface normal between the white and pial layer) were defined using *mri_vol2surf* in Freesurfer. This resulting fMRI data was then normalised to *fsaverage* using the transform defined from the PSIR data (see Figure 2, dashed lines path).

3.3.3 | Visualisation of normalised data

Note, for visualisation of volume normalised data, we utilised an optimal MNI 152 to fsaverage mapping strategy (Wu et al., 2018). Data from both normalisation streams were additionally displayed on a flattened representation of fsaverage, calculated by making cuts to the cortical surface and using a cost function to metrically optimise (in terms of distance) the flattened representation (available as standard in Freesurfer). A tool to aid visualisation of the flattened maps, used in this manuscript, is freely available at (https://github.com/KevinAquino/freesurferFlatVisualization.git).

3.4 | Smoothing of functional data

fMRI data in both volume and surface normalised space, were spatially smoothed (Figure 2, smoothed [S] shown by red lines) using a kernel of FWHM of 4.5 mm. In the volume stream, this is equivalent to applying a 3D Gaussian kernel; in the surface stream, the data were smoothed across the surface over a ring that corresponds to a kernel of 4.5 mm diameter at each vertex.
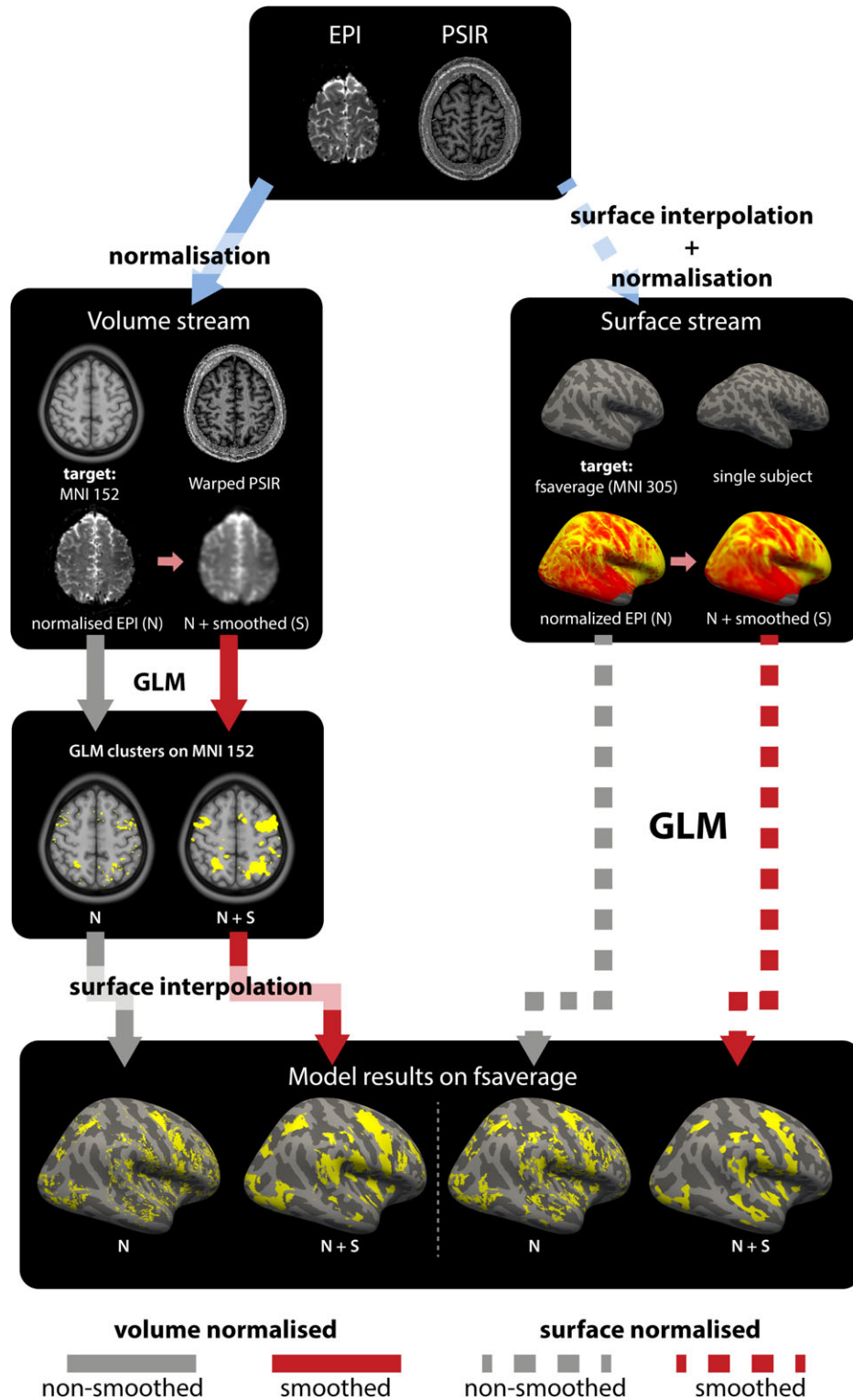
FIGURE 2 Schematic showing the main processing pipelines of fMRI data using volume normalisation (left stream) and surface normalisation (right stream). It should be noted that in both streams, there is a trilinear interpolation from volume to surface space. Clusters shown are those in response to the task for a single subject using a standard GLM, $p < .05$ FWE. Note, that in the figure N denotes normalised EPI data and S denotes smoothed data [Color figure can be viewed at wileyonlinelibrary.com]

3.5 | Functional MRI post-processing

3.5.1 | Individual subject general linear model design

Since the main focus of this work was to localise brain regions recruited by top-down modulation, the attention period (aISI) during each trial was modelled in the general linear model (GLM) for each

subject. All trials were modelled as all subjects showed performance greater than 70% accuracy in all conditions and we wanted to maximise statistical power in BOLD analyses. For each of the four conditions (i.e., one combination of S/V), the aISI time periods of each trial were set up as blocks and convolved with the standard
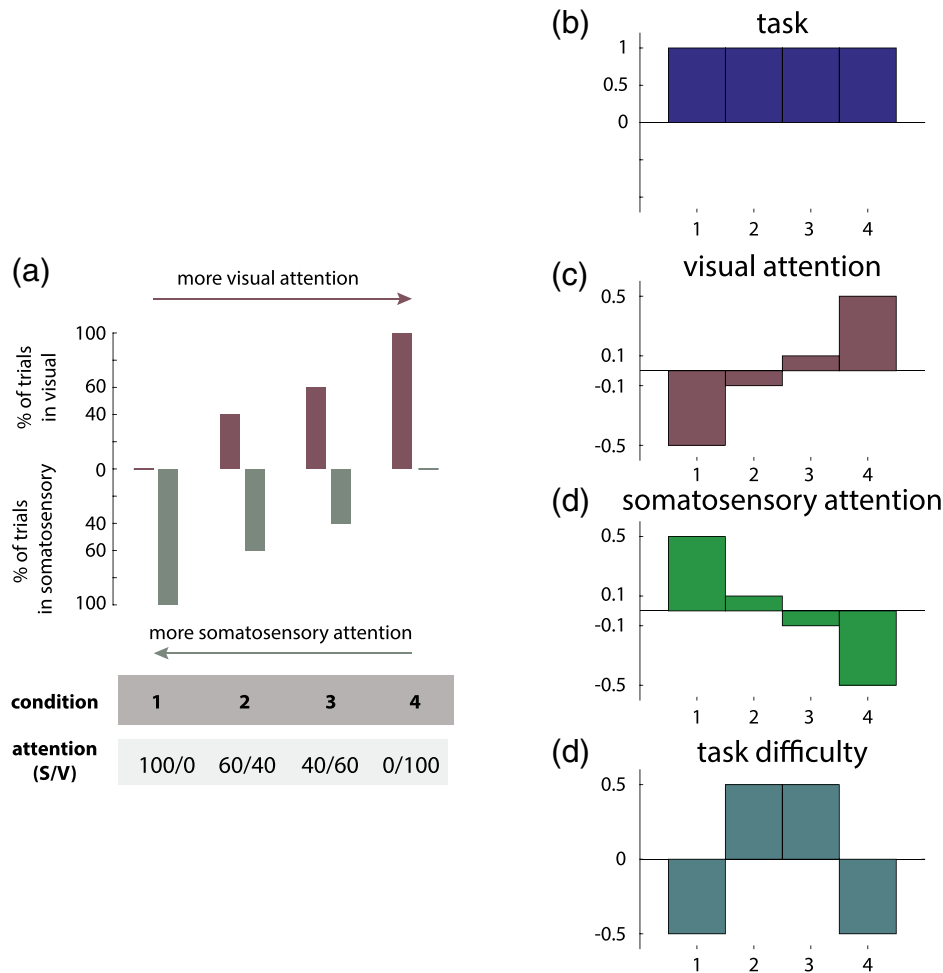
FIGURE 3 Schematic showing the different contrast conditions used in the first level GLM analysis. (a) The % of trials in the somatosensory/visual domain for each of the conditions. (b–e) The different contrasts used in the GLM analysis to interrogate the effects of attention [Color figure can be viewed at wileyonlinelibrary.com]

haemodynamic response function for each relevant software package (SPM or Freesurfer), Figure 1b, bottom panel. Although the standard HRFs differ slightly between packages, since we used a block design task, the convolution results in the predicted responses being invariant to any such small differences in HRF shape. This was repeated across the four fMRI runs resulting in 16 model estimates as regressors in a first level design matrix. In addition, the motion parameters were included as covariates of no interest and a constant term for each run to model differences in baseline GE-EPI signal between runs.

3.5.2 | Functional contrasts

Contrasts were assessed in a first level analysis and individual subject beta-weight (β) values computed. The contrasts assessed are summarised in Figure 3. They comprised: (i) a task contrast (Figure 3b) weighting all attentional conditions equally – to probe any brain regions recruited by the task independent of attentional cue; (ii) a positive linear contrast (Figure 3c) – to identify regions whose BOLD response linearly co-varied with increasing visual attention; (iii) a negative linear contrast (Figure 3d) – to identify regions whose BOLD response linearly co-varied with increasing somatosensory attention; and (iv) a task difficulty contrast (Figure 3e), using an 'n' shape to weight the 'hard' conditions (S/V 40/60 or 60/40) more than the

'easy' conditions (S/V 100/0 or 0/100) – to identify regions whose BOLD response was modulated by the division of attention between modalities, independent of where the attention was directed.

A one-sample *t*-test was used to threshold the maps for each functional contrast, which were then corrected for multiple comparisons. For volume normalised data, this correction was calculated using random field theory via the formulation of resolution elements (RESEL), as implemented in SPM12 (Worsley et al., 1996). For surface normalised data, RESELS are not simply described analytically (Hagler, Saygin, & Sereno, 2006), thus Monte Carlo simulations were used to generate an equivalent estimation (Hagler et al., 2006), as implemented in Freesurfer v.6.0.

3.5.3 | Atlas definition

To interrogate functionally specific regions, two functional cortical atlases were used. The Glasser atlas (as shown in Figure 4) comprising 180 regions per hemisphere, based on data from multimodal imaging (HCP-MMP 1.0) (Glasser et al., 2016), and the Freesurfer Destrieux Atlas (2009) (Destrieux, Fischl, Dale, & Halgren, 2010). These two atlases were applied to the normalised *fsaverage* brain (Freesurfer v 6.0) (see 'Subject normalisation') and on individual subject surface reconstructions for spatial interrogation of fMRI responses. Figure 4
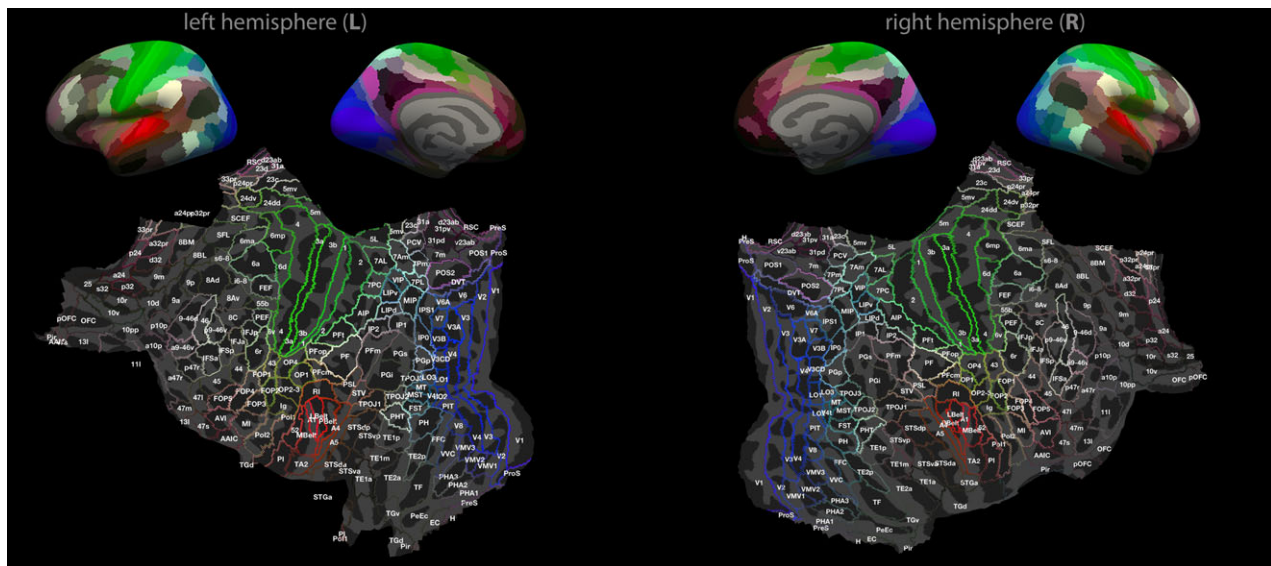
FIGURE 4 The relationship between the whole inflated brain (top row) and the Glasser atlas overlaid on the flattened patches (bottom row) – Note colours on the inflated brains correspond with the line colours on the flattened patches demarcating anatomical boundaries. Labels written on the flattened patches are taken from the Glasser atlas (Glasser et al., 2016) [Color figure can be viewed at wileyonlinelibrary.com]

shows the flattened representation, with region labels, that is used throughout the results and discussion sections.

3.6 | Group level fMRI analyses

One of the key benefits of UHF fMRI is the ability to extract highly sensitive and focal functional responses; however, this means that care must be taken to ensure optimal normalisation methods and smoothing is performed when grouping together subjects. Hence, here functional results are analysed at the group level using three different methods to demonstrate these issues and provide an optimal solution.

Method 1 was performed in both volume and surface normalised space, for both unsmoothed and smoothed data (see Figure 2). This method combined the corrected (p < .05, FWE corrected) one-sample t-test maps from each individual subject to form functional inter-subject conjunction maps. First, surviving voxels/vertices in the first level maps were used to form binary maps for each subject. These binary maps were then summed resulting in functional inter-subject conjunction maps ranging from 0 to 10 (representing each subject). This method was used to interrogate the spatial overlap for different normalisation methods (volume vs. surface), as well as the ability of spatial smoothing to increase subject overlap.

Method 2 involved analysis of the surface normalised, unsmoothed data (the winning pipeline from Method 1 – see Figures 8 and 9) using the 180 parcellated regions defined by the Glasser atlas (Glasser et al., 2016) to address the issue of poor subject overlap of higher-order cognitive regions (see Figure 8). Within each parcel and for each subject, the vertices with the top 5% of t-statistical values in response to the 'all' task condition were found to create the region of interest for that subject. The average β values for each condition for the vertices within the region of interest computed. These β values were then normalised across conditions (using the maximum β value of any condition) for each subject. Performing this analysis in surface

normalised space ensured that the same number of data points was used per subject for a given region. The dependence of the normalised β values on visual attention (or decreasing somatosensory attention) was then modelled for each of the 180 parcellated regions. Three candidate models were tested to match contrasts used in the GLM analyses (as shown in Figure 3): a constant model (task), a linear model (modality specific attention) and a negative quadratic (task difficulty) model. The 'winning' model was selected to be that which minimised the Bayesian Information Criterion (BIC) – a metric that 'rewards' model fit and 'punishes' model complexity (Schwarz, 1978). This metric was used to relatively compare model performance, as is performed in model fitting routines such as Dynamic Causal Modelling (Penny, 2012). The resulting analysis in the Glasser atlas regions within a given hemisphere were then corrected for false discovery rate (FDR) at a q-factor 0.1, thus allowing issues related to poor subject overlap to be explored with this sample size.

Method 3 performed a standard second level group GLM analysis on the volume normalised smoothed data (see Figure 2, red solid lines). The summary statistic from each contrast for the first level GLM analysis was used to perform a one-sample t-test in a conventional second level mixed effects GLM analysis. Finally, this method was used to demonstrate the manifestation of poor subject overlap – which can be predicted from the results of *Method 1*.

3.7 | Overlap metrics

In order to quantify the level of overlap in group-wise conjunction maps we compute an aggregate Dice coefficient. This was calculated by taking the Dice similarity index between two subjects i and j:

$$D_{i,j} = \frac{2|C_i \cap C_j|}{|C_i| + |C_j|}$$

where, C is the binarized threshold map (computed for Method 1 and 2) projected onto the surface template, $\cap$ indicates set intersection and

|| indicates cardinality. The average of the upper triangle matrix D_{ij} is used as a measure of the average subject overlap and is referred to as $\bar{D}$. In this formulation, a Dice coefficient of 1 indicates perfect overlap, and 0 indicates no overlap.

3.8 | Retinotopy analysis

Retinotopic maps were derived and visualised on surface and flattened representations (as detailed in the 'Normalisation' section) in order to validate the functional relationship to the structural, atlas based, cortical parcellation used. The data from the two retinotopic paradigms: the rotating wedges and the expanding/contracting annuli, were analysed to map visual polar angle and eccentricity, respectively. The data were processed with standard retinotopic analyses using mrTools. Following motion correction and co-registration, the scans from the wedge paradigm were combined: first, scans from both the clockwise and counter-clockwise condition were shifted by 2 frames, then the order of the volumes of the scans from the counter-clockwise condition were reversed prior to averaging with the scans form the clockwise condition. This reversal and shift was used to cancel out the effects from the spatiotemporal haemodynamic response function (Aquino et al., 2012). Following this average, the time series at each point were correlated with a cosine function with frequency that matched the stimulus delivery. The analysis provides a correlation – which indicates model fit, and a phase angle – which was correlated to the phase when the stimulus was presented and thus visual polar angle. Voxels that survived a correlation threshold of 0.4 were analysed for their phase. Half the visual hemifield contained phases that ranged from $[0,\pi]$ whereas the other half ranged from $[\pi,2\pi]$. Boundaries where the phase reversed were interpreted as borders of visual areas (Engel et al., 1994; Schira, Tyler, Breakspear, & Spehar, 2009). A similar procedure was repeated for the annuli paradigm, where the phase maps $[0,2\pi]$ were used as additional validation of a visual area.

4 | RESULTS

4.1 | Subject behavioural performance

Figure 5 shows the group mean behavioural responses to the task and indicates clear modulation of task performance, both accuracy and reaction time, across cue conditions. We show a significant ($p < .05$, three-way repeated measures ANOVA) effect of the cue condition on both accuracy ($p = 9 \times 10^{-9}$; $F = 400.1$) and reaction time ($p = 4.9 \times 10^{-10}$; $F = 771.5$). Lower accuracy (Figure 5a) and longer reaction times (Figure 5b) were observed for the trials when subjects divided their attention (40/60 and 60/40 cue conditions) compared with when subjects focused their attention on one modality (0/100 and 100/0 cue conditions). We also observed a significant effect of modality on accuracy ($p = 1.9 \times 10^{-4}$; $F = 36.5$) and reaction time ($p = 5 \times 10^{-9}$; $F = 456.1$), such that somatosensory attention modulated reaction times by a greater amount than visual attention. This was reflected by a significant cue × modality interaction for reaction time ($p = 1.4 \times 10^{-8}$; $F = 362.2$), with significantly shorter reaction times to somatosensory stimuli than visual stimuli (Figure 5b). In addition, a
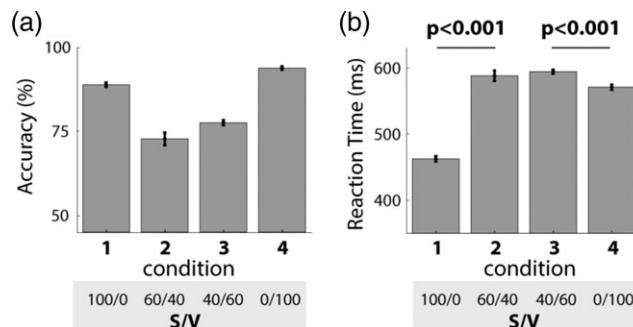

FIGURE 5 Group mean behavioural responses for (a) accuracy and (b) reaction time. A significant (three-way repeated measures ANOVA, $p < .05$) effect of cue, modality and subject on both accuracy and reaction time was observed. An interaction of cue and modality was observed for the reaction time, post-hoc t-test analyses reveal the differences (marked on b). Error bars indicate *SEM*

significant difference between subjects ($p = .014$; $F = 4.8$ and $p = 5.5 \times 10^{-4}$; $F = 4.8$, repeated measures ANOVA) in behavioural measures (accuracy and reaction time) was observed, demonstrating that all subjects did not perform the task equally, with some finding the paradigm more difficult than others.

4.1.1 | Anatomical variance

Figure 6 illustrates the greater inter-subject anatomical variability in both size and location of higher-order cognitive areas such as the IPS (Figure 6a), compared with the primary sensory regions such as the primary visual cortex (Figure 6b). Figure 6a,b show the atlas definitions of IPS and V1 on individual surfaces respectively, and the surface registered folding patterns (as indicated by the signed mean curvature K – a proxy for Sulci and Gyri as shown on the colour bar of Figure 6a,b). Across subjects, for the atlas defined IPS region, differences can be seen in the pattern of gyri (blue) and sulci (red) included with the region (highlighted with arrows in Figure 6a, bottom row). In particular, differences of the folding patterns inside, and in the neighbourhood of, the automated definition. The high quality of the surface normalisation procedure for all subjects in the primary visual cortex (V1), where there is less anatomical variability, can be verified by our retinotopy data (Figure 6c). This provided a functional map of visual region boundaries which showed strong spatial agreement with the Glasser atlas defined anatomical ROIs. Thus, these results implied two expectations for group functional analyses of focal responses (i) that primary sensory areas will have the highest overlap in functional maps (ii) higher order cortical areas – such as IPS and dorsal lateral prefrontal cortex (DLPFC) will have significantly lower functional overlap.

4.1.2 | Individual response to attention task

At the individual level, all subjects showed a significant ($p < .05$, FWE corrected) response to the task contrast condition (Figure 3b) and modulation to the cue condition, with the largest and most extensive responses generally seen for the task difficulty contrast condition (Figure 3e) with greater activation observed for the 40/60 conditions than the 0/100 conditions. However, the extent and location of the functional activation for each of the contrasts varied spatially across subjects relative to the structural information defined by the Glasser
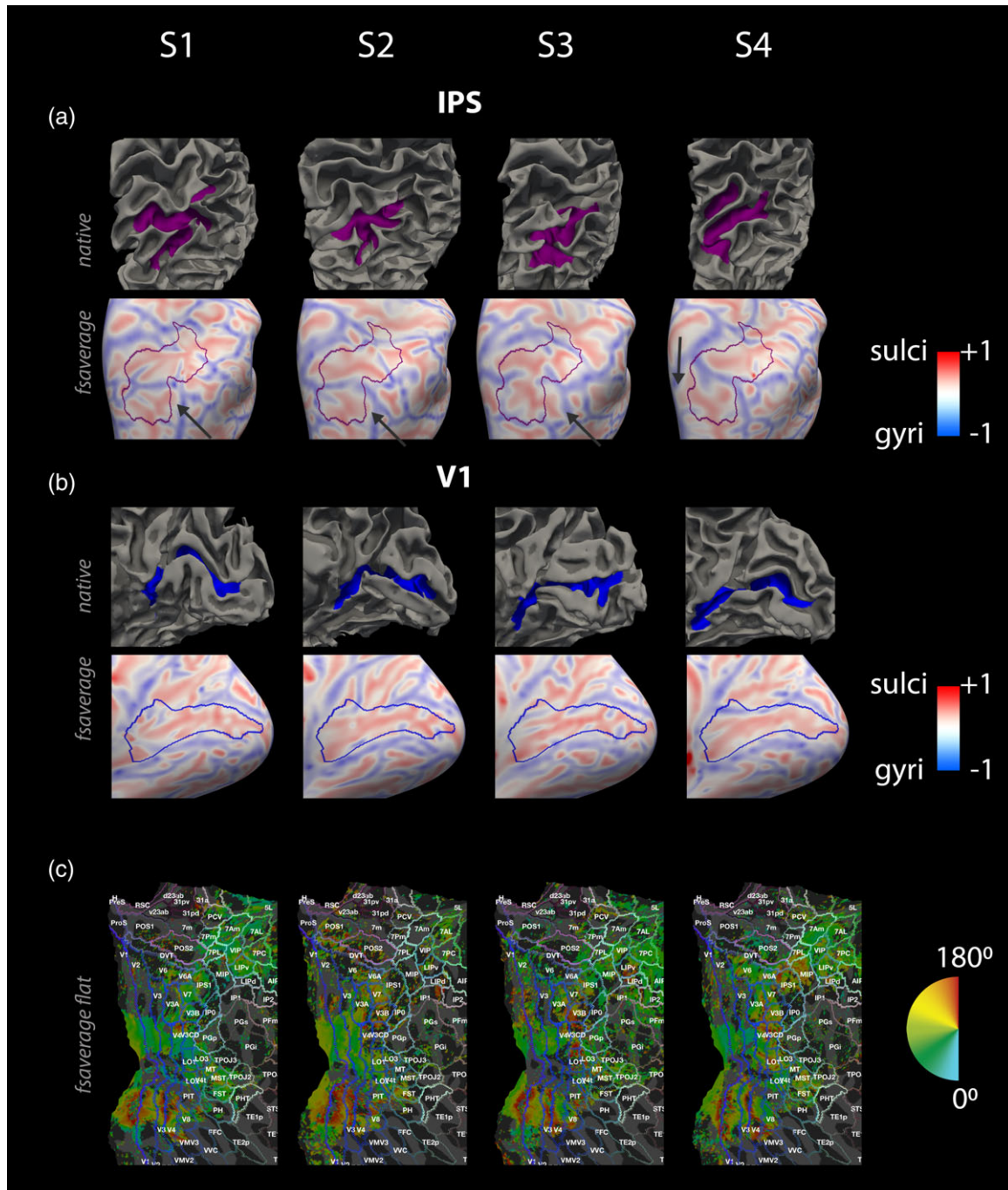
FIGURE 6 (a) Right IPS on native individual subject (S1–S4) surfaces (upper row, purple region shows IPS delineated by Freesurfer's registration method and Freesurfer Destrieux atlas), and on normalised space (lower row, IPS outlined in purple) where the individual subject curvature has been mapped into this space. Note the variability in the spatial pattern of sulci and gyri across subjects: There are clear differences in the anatomy (sulci shown in red, gyri shown in blue – Colour bar scales mean curvature) within the IPS boundary (purple line) between subjects, as highlighted by the arrows. (b) Data as for **a** shown for primary visual cortex (V1) demarcated in blue. Note the greater agreement of the sulci (shown in red) within V1 area across subjects in the normalised images. (c) Individual retinotopy on normalised flattened surface with the Glasser atlas overlaid. Note the retinotopy phase-reversals (corresponding to the left visual hemifield shown in the semicircle) denoting functional boundaries map onto the anatomically defined visual regions (V1–V3) [Color figure can be viewed at wileyonlinelibrary.com]

atlas (Figure 4), even when surface normalisation was used. Figure 7 illustrates this in two representative subjects, showing that whilst activation clusters to a given contrast were observed in approximately the same region, there was not exact spatial agreement across subjects, likely due to anatomical differences as well as the degree of functional response to the task.

It is worth noting that these individual responses contain focal units and have high statistical power using 4 runs of the experimental paradigm. Together, these results exemplify the power of using UHF for cognitive studies as the statistical power is high enough at the single subject level. The increased specificity however, means that variability in the anatomical location of functional activations is more
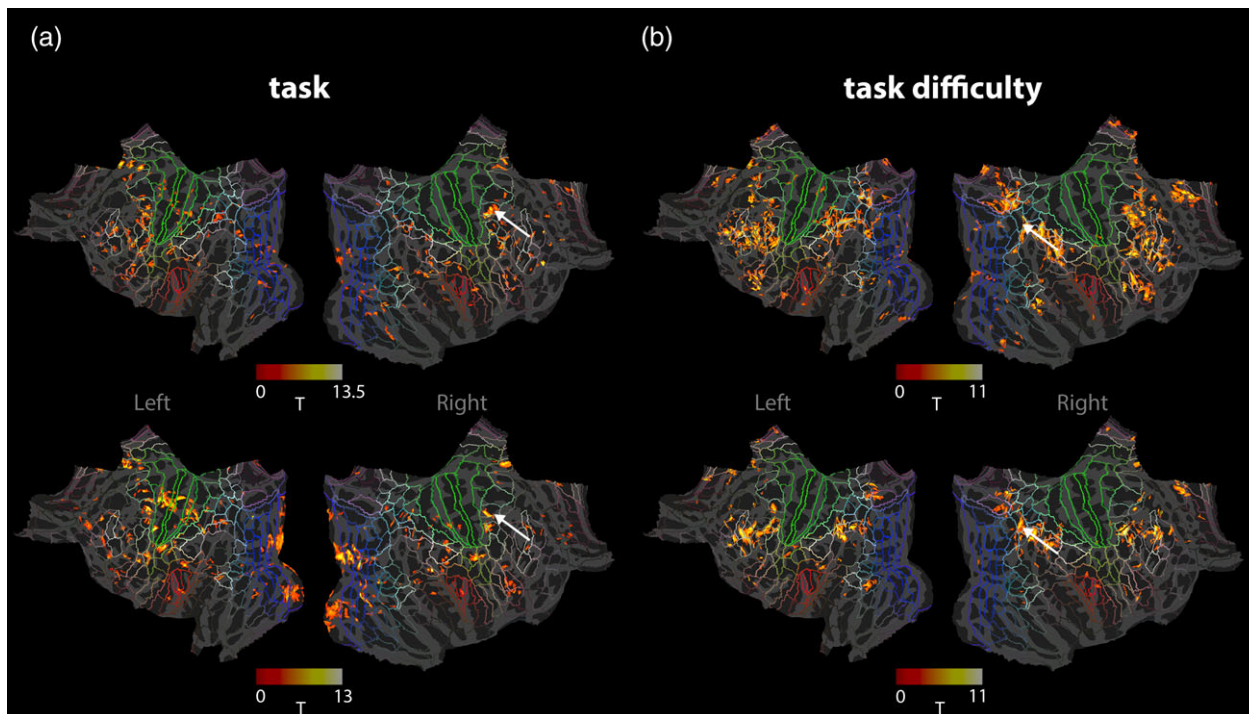
FIGURE 7 Maps showing regions of significant (*p* < .05, FWE corrected) activation to the *task* contrast (a) and *task difficulty* (b) contrast (see Figure 3b,e) for two subjects (top and bottom row, respectively). Individual subject maps have been surface normalised to the fsaverage template. Lines demarking anatomical regions are derived from the Glasser atlas, as shown in Figure 4. Arrows highlight variability of activity maps between subjects [Color figure can be viewed at wileyonlinelibrary.com]

significant at UHF than 3 T and this presents a challenge for group analyses.

4.1.3 | Surface versus volume normalisation

The effect of the spatial variability in functional responses is highlighted when analysing the data using *Method 1* when considering the normalisation of responses to a standard template and the effect of smoothing the data. Figure 8 compares the effect of volume and surface normalisation on the spatial agreement of significant areas of activation in response to the attention task paradigm across subjects. The importance of the choice of normalisation method can be seen by comparing the spatial overlap conjunction map of frontal-eye-field (FEF) and intraparietal sulcus 1 (IPS1) activations for volume (Figure 8b,d) and surface (Figure 8f,h) normalisation (see Figure 4 for region definitions). Volume normalisation results in poor inter-subject spatial agreement, with the overlapping activity in three or less subjects in FEF (Figure 8b) and IPS1 (Figure 8d), due to the focal nature of the responses combined with the observed anatomical variability in higher order cognitive areas (Figure 6a). A much greater spatial overlap was observed for surface normalisation (Figure 8a,f,h), with overlapping activity in up to seven subjects in the FEF (Figure 8f) and five in the IPS1 (Figure 8h). These differences are quantified in the region-specific Dice coefficient of spatial overlap (Figure 8j).

Spatial smoothing – a method to increase subject overlap as well as statistical power – also has profound effects on the inter-subject overlap of activations. The Dice coefficient computed over the entire right hemisphere is generally larger with spatial smoothing for both volume and surface normalisation methods, with the exception of task difficulty using surface normalisation (Figure 9a). However, it is

important to understand the overlap in focal regions, and this is shown by comparing Figure 8b,d with Figure 8c,e for volume normalisation, and Figure 8f,h with Figure 8g,i for surface normalisation, and quantified in Figure 8j. Applying spatial smoothing to the volume normalised data (Figure 8c,e) helped compensate for anatomical variability, especially in the FEF, but the resultant spatial agreement was still lower than for surface normalisation alone. Spatial smoothing of the surface normalised data reduced the spatial overlap in some areas such as the IPS1 and V3 (Figure 8g,i), since focal responses will be reduced when a smoothing kernel of greater extent than the activity is used. These differences are quantified by the region specific Dice coefficient (Figure 8j) which highlights that in most cases smoothing increased this overlap but not for regions that have focal activity – specifically regions in the early visual stream V1–V4, and higher order visual (an attention) areas V7, PEF, LIPv and LIPd. Similar effects were observed for the *task difficulty* contrast. Figure 9 illustrates the advantage of surface normalisation (Figure 9b) over volume normalisation (Figure 9a) for the detection of both the *task* contrast and *task difficulty* contrast across a group (see Supporting Information Figure S1 for inferior views of Figure 9). Figures 8 and 9 show that in general, response to task was observed in the visual stream from V1 to V4 and into the lateral intraparietal (LIP) region as well as in the FEF, whilst task difficulty correlated with activity of the IPS and dorsal lateral prefrontal cortex (also see Supporting Information Figure S2 top).

In addition, activations to the positive linear contrast (attention to visual domain) were observed, but these were far more focal than the task condition or task difficulty condition, resulting in little inter-subject spatial overlap (Supporting Information Figure S2 bottom), even when using the optimal pipeline of surface normalisation and no
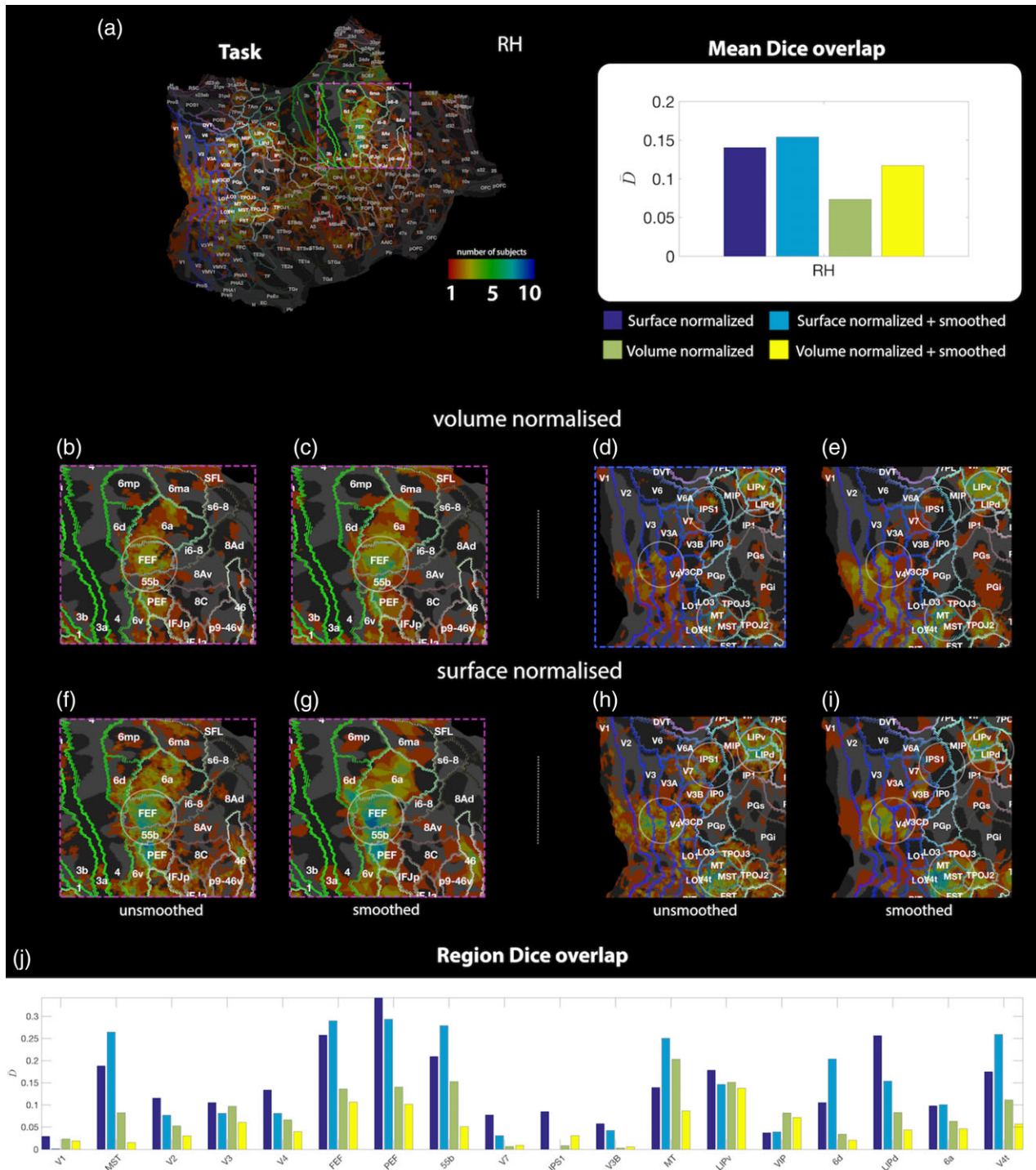
FIGURE 8   Comparison of group conjunction of individual subject T-stat maps (*p* < .05, FWE corrected) for the *task* contrast between different pre-processing pipelines using method 1. (a) Group conjunction map for the whole right hemisphere, created from the surface normalisation and no smoothing stream (see Figure 2, grey dashed line). Pink box includes frontal-eye-field area shown in Panels (b,c + f,g) whilst blue box includes the intraparietal cortex shown in Panels (d,e + h,i). Panels (b,d) show volume normalisation without spatial smoothing. Panels (c,e) show the volume normalisation with 4.5 mm FWHM spatial smoothing. Panels (f,h) show surface normalisation without smoothing, whilst Panels (g,i) show surface normalisation with 4.5 mm FWHM surface smoothing. Circles in Panels (b–i) draw attention to regions where conjunction of T-stat maps varies greatly dependent on the processing pipeline employed. (j) Region-specific Dice coefficients (*D*) of spatial overlap in selected key areas involved in the task. For similar maps for task difficulty condition and visual attention condition see Supporting Information Figure S2 [Color figure can be viewed at wileyonlinelibrary.com]

spatial smoothing. No significant activations to the negative linear contrast (attention to somatosensory domain) were seen consistently over the group, regardless of analysis stream.

4.1.4 | Assessment of attentional contrasts

To address the issue of poor subject overlap *Method 2* was employed using the optimal normalisation method (surface-registered and
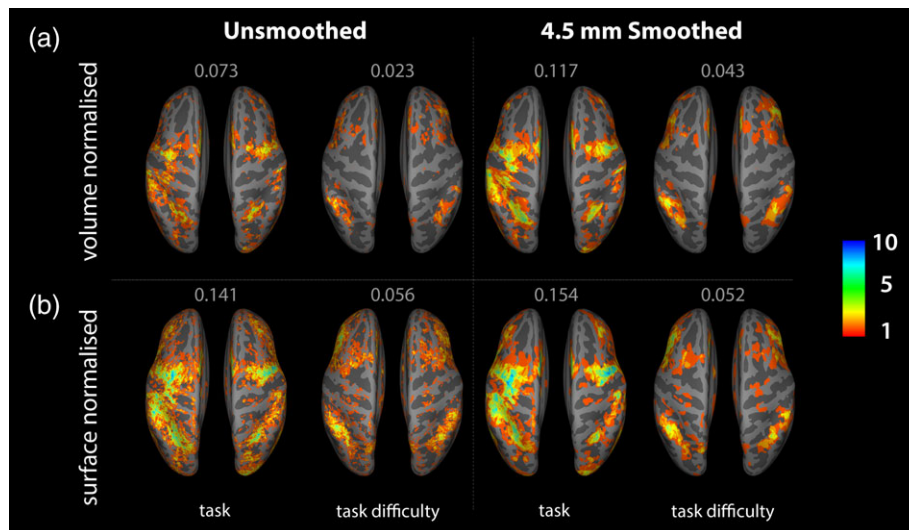
FIGURE 9 Group conjunction of individual subject T-stat maps (FWE *p* < .05) showing number of subjects with overlapping activation using the different processing pipelines of method 1. (a) Volume normalisation and (b) surface normalisation. For (a) and (b) results are shown for unsmoothed (left) and smoothed (4.5 mm FWHM kernel) data (right). The numbers in grey represent the mean dice overlap for both hemispheres for each contrast and processing stream. For inferior views, see Supporting Information Figure S1 [Color figure can be viewed at wileyonlinelibrary.com]

unsmoothed). Figure 10 shows the result of performing model fits (constant, linear or quadratic) to the individual subject normalised β values, across all four conditions, for each anatomical region of the Glasser atlas. This provided an alternative method to investigate those areas which showed a significant linear (i.e., increased visual or somatosensory domain attention) or 'n'-shape modulation (i.e., task difficulty) in response to the attention task. For a given anatomically defined region, statistical tests were performed only on voxels that responded to the task contrast (Figure 3b) in that parcel for each individual subject. A significant 'n'-shape correlation was found in a

number of regions (Figure 10a,b, blue), with large clusters of parcellated regions seen in the parietal and dorsal lateral prefrontal cortex. Significant linear correlations all showed a positive gradient (i.e., increased visual attention) and were seen in the visual cortex and VIP (Figure 10a,b, red-orange). The most robust linear modulations were seen in the Fusiform face complex (FFC) (*p* = .008, FDR corrected) with the strongest linear modulations of the lower-order visual areas (V1–V4) found in V4 (*p* = .06, FDR corrected) [V3: *p* = .09, FDR corrected]. The strongest 'n'-shaped modulation was seen in area 7 m (*p* = .002, FDR corrected) of parietal cortex and in Area 44 (*p* = .005,
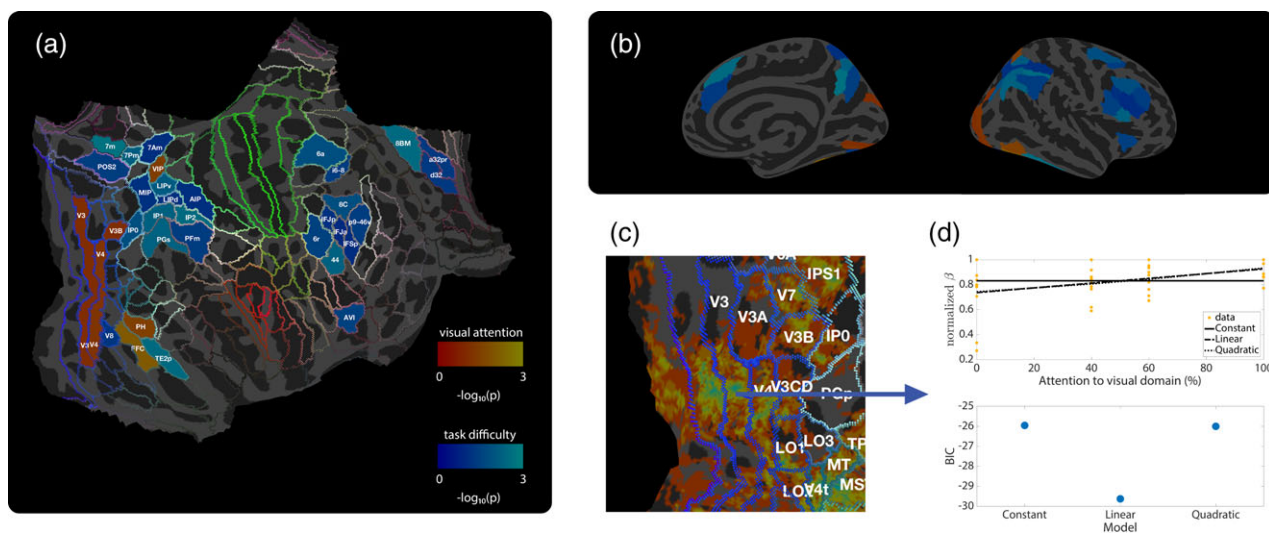

FIGURE 10 (a) The winning models (linear or quadratic, assessed with BIC) calculated across cortical regions using method 2 (FDR adjusted and threshold at *p* < .1); highlighting the regions showing linear modulation (red/orange, i.e., increased visual or somatosensory domain attention) and quadratic modulation (blue, i.e., 'n'-shape task difficulty). (b) Inflated views of the data shown in a. (c) Selected region of interest (V3) with group conjunction of response to task (akin to Figure 8a). (d) An example of a model fit (top panel) to the top 5% of b values from region V3, and the BIC calculated for the three candidate models, showing a linear fit clearly 'winning' in this region [Color figure can be viewed at wileyonlinelibrary.com]
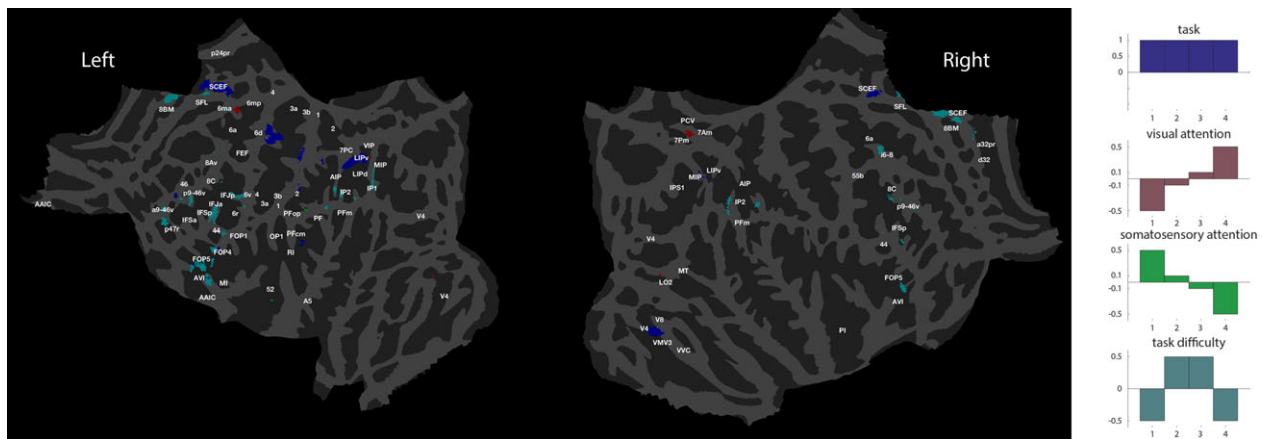
FIGURE 11 Second level GLM analyses of the volume normalised, smoothed attention data using method 3. Mixed effects analysis (*p* < .001, uncorrected) activation maps. Colours denote regions where the *t*-statistics for each of the contrasts exceeded the stated threshold, and were classified as 'activated' regions to that contrast, with different contrast and associated colours shown in right hand panel [Color figure can be viewed at wileyonlinelibrary.com]

FDR corrected) of dorsal lateral prefrontal cortex. An example region of interest, V3, and its model fit are shown in Figure 10c,d, respectively.

4.1.5 | Standard group analysis

The poor subject overlap, implied that group effects using standard analyses as described by *Method 3* will be weak, and this is shown in Figure 11 using a standard mixed effects group analysis results for the attention task. This highlights that standard methods do not readily reveal the modulations of the functional responses to this cognitive task even when using a relatively lenient threshold of *p* < .001, uncorrected. Focusing on the right hemisphere responses, as stimuli were presented to the left; we observed that, whilst some areas showed the response to task regardless of the attentional cue (Figure 10, dark blue), only very small disparate areas showed activation to the task difficulty (quadratic, shown in pale blue) or attention to a modality (linear, positive – shown in red, negative – shown in green) across the conditions. This lack of response was due to lack of spatial agreement across subjects (see Figures 6, 8 and 9) and highlights the need for optimal analysis pipelines to investigate such responses in high spatial resolution fMRI data. Additional activations observed in the left hemisphere are related to the button press response and the response to the task, rather than the direction of attention and therefore were not the focus of this study.

5 | DISCUSSION

We explored the feasibility of using high spatial resolution UHF fMRI to interrogate the BOLD response to a cognitive task across the whole brain. We show high quality whole brain data is achievable (see Supporting Information Material for magnetic field inhomogeneity [ΔB_0] and temporal SNR data). We then explored the inter-subject differences in brain structure in both primary visual areas and higher-order cortical regions and its likely contribution to inter-subject differences in the spatial location of functional responses. We showed that considerable differences in anatomy are present in higher order

cortical areas, whilst primary visual regions showed good anatomical agreement, as published previously (Fischl et al., 2008).

Given the observed inter-subject structural and functional differences, we investigated the effect of normalisation and smoothing procedures on the spatial agreement of the functional response to the cognitive task, in particular in higher order areas. We show that the choice of normalisation and smoothing procedures employed is critical when the fMRI response of interest is focal and/or in higher-order cortical regions. We demonstrate a novel group fMRI analysis for assessing attentional modulation to the cognitive task, by fitting β weights derived from first level GLM analysis to different models within each parcellated region. We reveal areas which show quadratic and linear modulations of BOLD signal in response to the attention conditions of the task, findings which are not clearly observed using standard second level mixed effects GLM analysis due to the large inter-subject spatial variability and difference in amplitude of functional response modulations.

5.1 | Data quality, anatomical variability and parcellation of brain regions

When considering whole brain functional responses, it is important to first consider the GE-EPI data quality. We used IB-shimming and B_0 mapping to provide good global B_0 homogeneity for the attention fMRI data acquisition, this ensured a subvoxel shift of pixels in the GE-EPI data in the phase encode direction compared with the anatomical data (Supporting Information Figure S3 and Supporting Information Text). In future we will improve this further with the use of dynamic distortion correction techniques (Visser, Poser, Barth, & Zwiers, 2012). tSNR was also relatively homogeneous over the cortex (Supporting Information Figure S4 and Supporting Information Text), though there was a noticeable reduction in the temporal lobes, regions known to be most greatly affected by physiological noise (Hutton et al., 2011) and to be the greatest distance from the receive coils, and the central gyrus driven by a reduced mean signal caused by heavy myelination in this region (Glasser & Van Essen, 2011).

Group analysis of fMRI data typically requires data normalisation to interrogate all subjects' data in the 'same space' and to allow the study of responses in equivalent regions. Given the known anatomical variability between subjects (Geyer et al., 2011), it is questionable whether normalisation of data to a standard template is appropriate using any transformation (i.e., volume or surface normalisation). However, a method of parcellating the brain, or defining anatomical structures, is necessary to form group comparisons. In the absence of individual subject sub-millimetre anatomical scans of multiple MR contrasts for parcellation of brain structures (Tardif et al., 2015), surface normalisation with a detailed anatomical atlas, such as the Glasser atlas (Glasser et al., 2016), may be the best approach.

Surface normalisation approaches match the curvature of the sulci and gyri of individual subjects to a template. In a recent study, Tardif et al demonstrate that surface based methods can be refined to improve spatial normalisation based on such curvature (Tardif et al., 2015). However, they also highlight that it may not be beneficial to maximise normalisation based on curvature and cortical folds, since in higher cortical areas, the curvature may not reflect the functional boundaries of regions (Tardif et al., 2015). Instead, they suggest information is required to allow alignment of individual brains based on functional boundaries. These functional boundaries are commonly believed to be reflected by cytoarchitecture, but it is not possible to interrogate cytoarchitecture directly in vivo. Instead, T_1 maps may provide additional information on myelination, which is believed to closely relate to cytoarchitecture, to inform group normalisation (Tardif et al., 2015; Turner & Geyer, 2014) or allow parcellation of individual brain regions (Geyer et al., 2011; Turner & Geyer, 2014). However, the success of this form of normalisation has primarily been assessed on myelin rich primary sensory cortices. Whilst some gains have been highlighted in higher order regions, FEF and ventral intra-parietal area (VIP) (Tardif et al., 2015), it remains to be assessed as to how useful this normalisation is for other higher cortical regions, where myelination is generally lower with less contrast between regions. Indeed, it is unclear whether whole brain normalisation based on T_1 maps may bias warping of the brain to correctly align regions of high myelin at the expense of functional areas with low myelin. Our data highlights the importance of future developments to map functional boundaries in individual subjects in vivo, to enable subject-specific structural and functional parcellation (Geyer et al., 2011; Robinson et al., 2017). Such boundary alignment may also take account of boundaries identified from robust fMRI tasks, such as individual subject resting state and visuotopic maps, as employed by Glasser et al. (2016). With such subject specific parcellations, β weights could be extracted from individual subject anatomical/functional regions and fed into a fitting process as used here (Turner & Geyer, 2014). Alternatively, the landmarks of individual subject borders may be used to provide a more accurate normalisation, as suggested by Tardif et al. (2015), subsequently allowing more standard GLM approaches to be employed. However, it should be noted that such additional measures to define structural or functional boundaries in an individual subject come at the expense of considerable addition scan time. Further, it should be noted that although surface-based normalisation techniques are optimal for maximising cortical activation

overlap, volume normalisation is still necessary when studying subcortical structures.

5.2 | Spatial smoothing

Spatial smoothing of fMRI data is widely adopted at lower field strength to blur inter-subject structural differences in brain anatomy for group analyses, increase statistical power (Turner & Geyer, 2014), and ensure data meets Gaussian Random Field theory assumptions for statistical analysis (Worsley & Friston, 1995). Until recently, many UHF whole brain studies have employed considerable spatial smoothing (Boyacioglu et al., 2014; Goodman et al., 2017; Mestres-Misse et al., 2017). In a recent study,(Torrisi et al., 2018) showed there is a substantial benefit for smoothing the data at 7 T using the same smoothing kernel at 3 T.

However, recent articles (e.g. Stelzer, Lohmann, Mueller, Buschmann, & Turner, 2014; Turner & Geyer, 2014; Turner, 2016]) highlight that the use of large smoothing kernels negates the benefits of the high spatial resolution of fMRI achievable at UHF. In addition, they highlight that smoothing is not required for False Discovery Rate correction (Turner & Geyer, 2014) due to the inherent smoothness of fMRI data due to the point-spread function of the BOLD response (Polimeni et al., 2017; Stelzer et al., 2014). Turner (Turner & Geyer, 2014) provides a detailed critique of the problems associated with spatial smoothing (Stelzer et al., 2014; Turner, 2016; Turner & Geyer, 2014). Here, we show the limitations of spatially smoothing high resolution fMRI data, highlighting that focal responses in higher-order areas can be diluted by smoothing to the point that these responses no longer survive statistical analyses, resulting in reduced overlap of activations across subjects (compare Figure 9h,i).

Without spatial smoothing, methods to best deal with differences in brain anatomy become vital to minimise inter-subject spatial variability, especially for higher-order cognitive areas for which anatomical variability is greater than for primary sensory areas (Turner & Geyer, 2014). Minimal anatomical variability in primary sensory cortex may, in part, explain the successes of UHF high spatial resolution studies of sensorimotor and visual cortex (Goncalves et al., 2015; Kemper et al., 2017; Poltoratski et al., 2017; Rua et al., 2017; Sanchez Panchuelo et al., 2015; Sanchez Panchuelo et al., 2016; Sanchez-Panchuelo et al., 2012). Indeed, our data confirmed this observation, showing good inter-subject correspondence of V1 (Figure 6b) and excellent correspondence of the anatomical and functional boundaries of V1–V3 (Figure 6c). However, anatomical agreement of higher-order areas, such as the IPS, was much poorer, with considerable variability across subjects observed even with the use of surface normalisation (Figure 6a).

5.3 | Limitations of group GLM analyses for cognitive tasks

Stelzer et al. (2014) have previously highlighted conceptually that fundamental differences in spatio-temporal representations of brain function leads to potential pitfalls when using a mixed effects GLM group analysis. They highlight that if the spatio-temporal pattern of response does not overlap completely across subjects, only a subset of the true activation for each individual will be present in the group analysis, that

is, the region where there is spatial agreement over subjects. This is due to both inter-subject anatomical differences and differences in functional brain activity due to the subjects' response to the task (i.e., relationship to the canonically modelled response) which is likely to be particularly prevalent in cognitive tasks where individual subject strategy may differ. As such, a standard second level mixed effects GLM can only ever provide a partial picture of the true functional response to a cognitive task, as has also previously been shown from ICA and MVPA analysis (Etzel, Zacks, & Braver, 2013; Xu, Potenza, & Calhoun, 2013).

Our results (Figure 11) corroborate the concerns raised in Stelzer's thought experiment, demonstrating that a standard second level GLM analysis results in little common activation observed to any contrast (response to task, attention to visual stimuli, attention to somatosensory stimuli or task difficulty). This is due to the lack of precise spatial agreement between subjects (Figures 8 and 9; Supporting Information Figure S1), despite use of a liberal $p < .001$ uncorrected threshold and spatial smoothing. Whilst the extent of responses are increased using a fixed effects analysis, with a response to both the task contrast and task difficulty contrast observed (dark blue and pale blue), no linear modulations are seen. Therefore we propose that standard GLM approaches are not best suited to studies where functional responses are likely to vary across subjects due to task complexity and different task completion strategies.

5.4 | Functional interpretation of responses to attention paradigm

Tasks focussed on the direction of spatial attention to somatosensory stimuli have previously elicited responses in the inferior parietal lobe (IPL), FEF and SII (Wu et al., 2014). Similarly the FEF and IPS, as well as posterior parietal cortex, cingulate, striate and extrastriate cortex (Corbetta et al., 2000; Martinez et al., 1999) have been shown to be active in response to visual spatial attention (Corbetta et al., 2000; Martinez et al., 1999). The attention related activations in the parietal and DLPFC regions (Figure 10) to sensory modality that we report using our optimised analysis pipeline are in line with previous observations. Here, we advance previous studies by varying the relative direction of attention between the visual and somatosensory domain, creating four conditions, whereas previous fMRI work has only directed attention in a binary fashion: from one location to another (spatial or modality). Such BOLD signal modulations between graded levels of attention are more subtle, requiring the higher CNR afforded by UHF fMRI.

We show that in parietal and DLPFC regions (Figure 10) the modulation related to attention level is quadratic, such that the fMRI BOLD response during the attention period is larger when attention is split between the two modalities (40/60 conditions) than when the attention is directed purely to one modality (0/100 conditions). This suggests that this attention effect is independent of the modality to which attention is to be directed and is instead related to task difficulty. This concept agrees with Macaluso et al. (2003), who report modality independent modulations in superior premotor areas, left inferior parietal lobule, posterior parietal and prefrontal cortices, and Corbetta et al. (2000) which attributes activity in the IPS to be purely related to the top-down process of attention, rather than the response to a stimulus.

The quadratic response to the direction of attention between modalities has been documented in our parallel EEG-study using the same paradigm (Sokoliuk et al. (2018)). In our four conditions we linearly increase visually-directed-attention with condition number (1–4, Figure 3c) whilst simultaneously linearly decreasing somatosensory-directed-attention with condition number (1–4, Figure 3d). Analysing these two contrasts is aimed at mapping the attentional changes within these two modalities. However in the Hard (40/60,60/40) > Easy tasks (0/100,100/0) this contrast resembles a quadratic function when formulated over the 4 conditions (Figure 3e) [as in Sokoliuk et al., 2018] with the shape reflecting variation in total attentional load.

Our paradigm also allows us to differentiate regions that are independent of the modality to which attention is directed, from those regions where the modulation of the BOLD response is dependent on the modality that attention is directed to. We observe a linear modulation, increasing BOLD fMRI signal with increasing visual attention, within extrastriate visual cortex areas of V3, V4, V3b, area Parietalis (temporo-occipital) Basalis (PH, [Von Economo & Koskinas, 1925; Triarhou, 2007; Glasser & Van Essen, 2011]), Fusiform face complex (FFC) and VIP. Previously, analogous linear modulations of brain activity with attention have been reported in EEG data where alpha power has been shown to linearly decrease in the occipital/parietal regions of the hemisphere to which increasing spatial visual attention has been paid (Gould et al., 2011). However, EEG does not have the spatial resolution to identify the precise anatomical region in which the alpha power modulation is observed.

Of the lower order visual areas (V1–V4), V4 showed the most robust linear modulation with attention. Invasive animal electrophysiology recordings provide compelling supporting evidence that our analyses are identifying neuronal modulation by attention, since in these studies spike–spike coherence in the alpha and gamma bands has been shown to be significantly modulated by directed spatial attention in V4, but not in V1 (Buffalo, Fries, Landman, Buschman, & Desimone, 2011). These invasive recordings showed that alpha power decreased when attention was directed to the visual area from which neuronal responses are measured. This report of a reduction in alpha power (Buffalo et al., 2011), negatively correlates with the observed increase in V4 BOLD response with increasing visual attention that was observed in this study, a finding supported by many previous electrophysiology reports of anti-correlation between alpha power and BOLD signals (e.g., Goldman, Stern, Engel, & Cohen, 2002; Laufs et al., 2006; Mayhew, Ostwald, Porcaro, & Bagshaw, 2013; Mullinger, Mayhew, Bagshaw, Bowtell, & Francis, 2014). It should be noted that the invasive recordings (Buffalo et al., 2011) also showed a concordant increase in gamma power in V4 but no significant gamma power change in V1. Previous reports show that gamma oscillations are generally thought to be most closely coupled to the BOLD response (Logothetis, Pauls, Augath, Trinath, & Oeltermann, 2001; Magri, Schridde, Murayama, Panzeri, & Logothetis, 2012), suggesting that gamma changes could be driving the observed BOLD modulations we report. To our knowledge there are only reports of linear modulation of alpha with the graded manipulation of attention during a pre-stimulus cue period (e.g., Gould et al., 2011) but equivalent studies of gamma responses have not yet been performed.

Interestingly, we observed no negative linear modulations of BOLD responses across conditions (reflecting increased attention to the somatosensory domain), contrary to what might have been expected in the secondary somatosensory system (Wu et al., 2014). Modulations in reaction time for attending 100% compared with 60% were larger when subjects attended to the somatosensory domain, than when attention was directed to the visual domain. Furthermore, the modulation of the accuracy measure between 100 and 60% was similar for both domains (no significant cue × modality interaction). Therefore the behavioural results strongly suggest it is unlikely that the subjects' attention to the somatosensory domain was not modulated by this task, despite the lack of BOLD response in the somatosensory brain area. Modulation of modality specific alpha power with spatial attention have previously been reported for both the visual and somatosensory system (e.g., Gould et al., 2011; Haegens et al., 2011; Haegens et al., 2012; Zumer et al., 2014), suggesting the processes behind directing spatial attention are not different for the two systems (visual and somatosensory). Further investigation is required to clarify the lack of responses in the somatosensory system to this type of attention paradigm where attention is divided between two modalities, rather than spatially.

5.5 | Study limitations and future work

We note that our small sample size influenced the strength of some of the statistics (FDR correction at $q = 0.1$ in Figure 10, $p < .001$ uncorrected maps in Figure 11); however, the responses on the individual level were strong and demonstrate the potential of UHF fMRI for subject specific brain mapping (see Figure 7). Future modelling and/or concurrent analyses of EEG responses will provide better models to probe activations.

Future studies may also benefit from the use of multi-variate pattern analysis (MVPA), which, by using spatial pattern recognition, has the potential to overcome some of the limitations of group GLM analyses (Turner & Geyer, 2014). The optimal strategies presented here, that is, surface normalisation and no spatial smoothing, should be considered to be complementary, providing an initial method to identify regions of interest on which MVPA can be performed. Furthermore, the methods presented in this study allow analyses on a smaller data set without the requirement for training and subsequent test data sets which can be challenging to obtain for complex cognitive tasks.

6 | CONCLUSION

This study shows the potential of 7 T to study whole brain individual subject BOLD fMRI responses to a cognitive task. The optimal strategy of surface normalisation, no spatial smoothing and the analysis of responses within defined parcellations is demonstrated to assess cognitive processing involved in directing attention between sensory domains.

ORCID

Kevin M. Aquino https://orcid.org/0000-0002-7435-0236

Rodika Sokoliuk https://orcid.org/0000-0003-1798-6657

Daisie O. Pakenham https://orcid.org/0000-0002-0311-3102

Rosa Maria Sanchez-Panchuelo https://orcid.org/0000-0002-9917-0020

Simon Hanslmayr https://orcid.org/0000-0003-4448-2147

Stephen D. Mayhew https://orcid.org/0000-0003-1240-1488

Karen J. Mullinger https://orcid.org/0000-0002-8164-0274

Susan T. Francis https://orcid.org/0000-0003-0903-7507

REFERENCES

Aquino, K. M., Schira, M. M., Robinson, P. A., Drysdale, P. M., & Breakspear, M. (2012). Hemodynamic traveling waves in human visual cortex. *PLoS Computational Biology*, *8*(3), e1002435.

Avants, B. B., Tustison, N., & Song, G. (2009). Advanced normalization tools (ANTS). *Insight Journal*, *2*, 1–35.

Avants, B. B., Tustison, N. J., Song, G., Cook, P. A., Klein, A., & Gee, J. C. (2011). A reproducible evaluation of ANTs similarity metric performance in brain image registration. *NeuroImage*, *54*(3), 2033–2044.

Besle, J., Sanchez-Panchuelo, R. M., Bowtell, R., Francis, S., & Schluppeck, D. (2014). Event-related fMRI at 7T reveals overlapping cortical representations for adjacent fingertips in S1 of individual subjects. *Human Brain Mapping*, *35*(5), 2027–2043.

Boyacioglu, R., Schulz, J., Muller, N. C., Koopmans, P. J., Barth, M., & Norris, D. G. (2014). Whole brain, high resolution multiband spin-echo EPI fMRI at 7 T: A comparison with gradient-echo EPI using a color-word Stroop task. *NeuroImage*, *97*, 142–150.

Buffalo, E. A., Fries, P., Landman, R., Buschman, T. J., & Desimone, R. (2011). Laminar differences in gamma and alpha coherence in the ventral stream. *Proceedings of the National Academy of Sciences of the United States of America*, *108*(27), 11262–11267.

Carrasco, M. (2011). Visual attention: The past 25 years. *Vision Research*, *51*(13), 1484–1525.

Corbetta, M., Kincade, J. M., Ollinger, J. M., McAvoy, M. P., & Shulman, G. L. (2000). Voluntary orienting is dissociated from target detection in human posterior parietal cortex (vol 3, pg 292, 2000). *Nature Neuroscience*, *3*(5), 521–521.

De Martino, F., Moerel, M., Ugurbil, K., Goebel, R., Yacoub, E., & Formisano, E. (2015). Frequency preference and attention effects across cortical depths in the human primary auditory cortex. *Proceedings of the National Academy of Sciences of the United States of America*, *112*(52), 16036–16041.

De Martino, F., Yacoub, E., Kemper, V., Moerel, M., Uludag, K., de Weerd, P., … Formisano, E. (2017). The impact of ultra-high field MRI on cognitive and computational neuroimaging. *NeuroImage*, *168*, 366–382.

Destrieux, C., Fischl, B., Dale, A., & Halgren, E. (2010). Automatic parcellation of human cortical gyri and sulci using standard anatomical nomenclature. *NeuroImage*, *53*(1), 1–15.

Engel, S. A., Rumelhart, D. E., Wandell, B. A., Lee, A. T., Glover, G. H., Chichilnisky, E. J., & Shadlen, M. N. (1994). fMRI of human visual cortex. *Nature*, *369*(6481), 525.

Etzel, J. A., Zacks, J. M., & Braver, T. S. (2013). Searchlight analysis: Promise, pitfalls, and potential. *NeuroImage*, *78*, 261–269.

Fischl, B., Rajendran, N., Busa, E., Augustinack, J., Hinds, O., Yeo, B. T., … Zilles, K. (2008). Cortical folding patterns and predicting cytoarchitecture. *Cerebral Cortex*, *18*(8), 1973–1980.

Fischl, B., Sereno, M. I., & Dale, A. M. (1999). Cortical surface-based analysis. II: Inflation, flattening, and a surface-based coordinate system. *NeuroImage*, *9*(2), 195–207.

Fischl, B., Sereno, M. I., Tootell, R. B. H., & Dale, A. M. (1999). High-resolution intersubject averaging and a coordinate system for the cortical surface. *Human Brain Mapping*, 8(4), 272–284.

Fracasso, A., Luijten, P. R., Dumoulin, S. O., & Petridou, N. (2017). Laminar imaging of positive and negative BOLD in human visual cortex at 7T. *NeuroImage*, 164, 100–111.

Gardner, J. L., Merriam, E. P., Movshon, J. A., & Heeger, D. J. (2008). Maps of visual space in human occipital cortex are retinotopic, not spatiotopic. *Journal of Neuroscience*, 28(15), 3988–3999.

Geyer, S., Weiss, M., Reimann, K., Lohmann, G., & Turner, R. (2011). Microstructural parcellation of the human cerebral cortex - from Brodmann's post-mortem map to in vivo mapping with high-field magnetic resonance imaging. *Frontiers in Human Neuroscience*, 5, 19.

Gitelman, D. R., Nobre, A. C., Parrish, T. B., LaBar, K. S., Kim, Y. H., Meyer, J. R., & Mesulam, M. M. (1999). A large-scale distributed network for covert spatial attention - further anatomical delineation based on stringent behavioural and cognitive controls. *Brain*, 122, 1093–1106.

Glasser, M. F., Coalson, T. S., Robinson, E. C., Hacker, C. D., Harwell, J., Yacoub, E., ... Van Essen, D. C. (2016). A multi-modal parcellation of human cerebral cortex. *Nature*, 536(7615), 171–178.

Glasser, M. F., & Van Essen, D. C. (2011). Mapping human cortical areas in vivo based on myelin content as revealed by T1- and T2-weighted MRI. *The Journal of Neuroscience*, 31(32), 11597–11616.

Glover, G. H., Li, T. Q., & Ress, D. (2000). Image-based method for retrospective correction of physiological motion effects in fMRI: RETROICOR. *Magnetic Resonance in Medicine*, 44(1), 162–167.

Goldman, R. I., Stern, J. M., Engel, J., & Cohen, M. S. (2002). Simultaneous EEG and fMRI of the alpha rhythm. *Neuroreport*, 13(18), 2487–2492.

Gomez-Ramirez, M., Hysaj, K., & Niebur, E. (2016). Neural mechanisms of selective attention in the somatosensory system. *Journal of Neurophysiology*, 116(3), 1218–1231.

Goncalves, N. R., Ban, H., Sanchez-Panchuelo, R. M., Francis, S. T., Schluppeck, D., & Welchman, A. E. (2015). 7 tesla FMRI reveals systematic functional organization for binocular disparity in dorsal visual cortex. *The Journal of Neuroscience*, 35(7), 3056–3072.

Goodman, A. M., Wang, Y., Kwon, W. S., Byun, S. E., Katz, J. S., & Deshpande, G. (2017). Neural correlates of consumer buying motivations: A 7T functional magnetic resonance imaging (fMRI) study. *Frontiers in Neuroscience*, 11, 512.

Gould, I. C., Rushworth, M. F., & Nobre, A. C. (2011). Indexing the graded allocation of visuospatial attention using anticipatory alpha oscillations. *Journal of Neurophysiology*, 105(3), 1318–1326.

Gu, J., & Kanai, R. (2014). What contributes to individual differences in brain structure? *Frontiers in Human Neuroscience*, 8, 262.

Haegens, S., Handel, B. F., & Jensen, O. (2011). Top-down controlled alpha band activity in somatosensory areas determines behavioral performance in a discrimination task. *The Journal of Neuroscience*, 31(14), 5197–5204.

Haegens, S., Luther, L., & Jensen, O. (2012). Somatosensory anticipatory alpha activity increases to suppress distracting input. *Journal of Cognitive Neuroscience*, 24(3), 677–685.

Hagler, D. J., Jr., Saygin, A. P., & Sereno, M. I. (2006). Smoothing and cluster thresholding for cortical surface-based group analysis of fMRI data. *NeuroImage*, 33(4), 1093–1103.

Hutton, C., Josephs, O., Stadler, J., Featherstone, E., Reid, A., Speck, O., ... Weiskopf, N. (2011). The impact of physiological noise correction on fMRI at 7 T. *NeuroImage*, 57(1), 101–112.

Kanai, R., & Rees, G. (2011). OPINION the structural basis of inter-individual differences in human behaviour and cognition. *Nature Reviews Neuroscience*, 12(4), 231–242.

Kemper, V. G., De Martino, F., Emmerling, T. C., Yacoub, E., & Goebel, R. (2017). High resolution data analysis strategies for mesoscale human functional MRI at 7 and 9.4T. *NeuroImage*, 164, 48–58.

Klein, A., Andersson, J., Ardekani, B. A., Ashburner, J., Avants, B., Chiang, M.-C., ... Hellier, P. (2009). Evaluation of 14 nonlinear deformation algorithms applied to human brain MRI registration. *NeuroImage*, 46(3), 786–802.

Kok, P., Bains, L. J., van Mourik, T., Norris, D. G., & de Lange, F. P. (2016). Selective activation of the deep layers of the human primary visual cortex by top-down feedback. *Current Biology*, 26(3), 371–376.

Laufs, H., Holt, J. L., Elfont, R., Krams, M., Paul, J. S., Krakow, K., & Kleinschmidt, A. (2006). Where the BOLD signal goes when alpha EEG leaves. *NeuroImage*, 31(4), 1408–1418.

Logothetis, N. K., Pauls, J., Augath, M., Trinath, T., & Oeltermann, A. (2001). Neurophysiological investigation of the basis of the fMRI signal. *Nature*, 412(6843), 150–157.

Macaluso, E., Eimer, M., Frith, C. D., & Driver, J. (2003). Preparatory states in crossmodal spatial attention: Spatial specificity and possible control mechanisms. *Experimental Brain Research*, 149(1), 62–74.

Magri, C., Schridde, U., Murayama, Y., Panzeri, S., & Logothetis, N. K. (2012). The amplitude and timing of the BOLD signal reflects the relationship between local field potential power at different frequencies. *Journal of Neuroscience*, 32(4), 1395–1407.

Martinez, A., Anllo-Vento, L., Sereno, M. I., Frank, L. R., Buxton, R. B., Dubowitz, D. J., ... Hillyard, S. A. (1999). Involvement of striate and extrastriate visual cortical areas in spatial attention. *Nature Neuroscience*, 2(4), 364–369.

Mayhew, S. D., Ostwald, D., Porcaro, C., & Bagshaw, A. P. (2013). Spontaneous EEG alpha oscillation interacts with positive and negative BOLD responses in the visual-auditory cortices and default-mode network. *NeuroImage*, 76(1), 362–372.

Mestres-Misse, A., Trampel, R., Turner, R., & Kotz, S. A. (2017). Uncertainty and expectancy deviations require cortico-subcortical cooperation. *NeuroImage*, 144(Pt A), 23–34.

Mougin, O., Abdel-Fahim, R., Dineen, R., Pitiot, A., Evangelou, N., & Gowland, P. (2016). Imaging gray matter with concomitant null point imaging from the phase sensitive inversion recovery sequence. *Magnetic Resonance in Medicine*, 76(5), 1512–1516.

Muckli, L., De Martino, F., Vizioli, L., Petro, L. S., Smith, F. W., Ugurbil, K., ... Yacoub, E. (2015). Contextual feedback to superficial layers of V1. *Current Biology*, 25(20), 2690–2695.

Mullinger, K. J., Mayhew, S. D., Bagshaw, A. P., Bowtell, R., & Francis, S. T. (2014). Evidence that the negative BOLD response is neuronal in origin: A simultaneous EEG-BOLD-CBF study in humans. *NeuroImage*, 94, 263–274.

Olman, C. A., Harel, N., Feinberg, D. A., He, S., Zhang, P., Ugurbil, K., & Yacoub, E. (2012). Layer-specific fMRI reflects different neuronal computations at different depths in human V1. *PLoS One*, 7(3), e32536.

Penny, W. D. (2012). Comparing dynamic causal models using AIC, BIC and free energy. *NeuroImage*, 59(1), 319–330.

Pohmann, R., Speck, O., & Scheffler, K. (2016). Signal-to-noise ratio and MR tissue parameters in human brain imaging at 3, 7, and 9.4 tesla using current receive coil arrays. *Magnetic Resonance in Medicine*, 75(2), 801–809.

Polimeni, J. R., Renvall, V., Zaretskaya, N., & Fischl, B. (2017). Analysis strategies for high-resolution UHF-fMRI data. *NeuroImage*, 168, 296–320.

Poltoratski, S., Ling, S., McCormack, D., & Tong, F. (2017). Characterizing the effects of feature salience and top-down attention in the early visual system. *Journal of Neurophysiology*, 118(1), 564–573.

Posner, M. I. (1980). Orienting of attention. *The Quarterly Journal of Experimental Psychology*, 32(1), 3–25.

Puckett, A. M., Bollmann, S., Barth, M., & Cunnington, R. (2017). Measuring the effects of attention to individual fingertips in somatosensory cortex using ultra-high field (7T) fMRI. *NeuroImage*, 161, 179–187.

Reithler, J., Peters, J. C., & Goebel, R. (2017). Characterizing object- and position-dependent response profiles to uni- and bilateral stimulus configurations in human higher visual cortex: A 7T fMRI study. *NeuroImage*, 152, 551–562.

Rihs, T. A., Michel, C. M., & Thut, G. (2007). Mechanisms of selective inhibition in visual spatial attention are indexed by alpha-band EEG synchronization. *European Journal of Neuroscience*, 25(2), 603–610.

Robinson, E. C., Garcia, K., Glasser, M. F., Chen, Z., Coalson, T. S., Makropoulos, A., ... Rueckert, D. (2017). Multimodal surface matching with higher-order smoothness constraints. *NeuroImage*, 167, 453–465.

Rua, C., Costagli, M., Symms, M. R., Biagi, L., Donatelli, G., Cosottini, M., ... Tosetti, M. (2017). Characterization of high-resolution gradient Echo and Spin Echo EPI for fMRI in the human visual cortex at 7T. *Magnetic Resonance Imaging*, 40, 98–108.

Sanchez Panchuelo, R. M., Ackerley, R., Glover, P. M., Bowtell, R. W., Wessberg, J., Francis, S. T., & McGlone, F. (2016). Mapping quantal

touch using 7 tesla functional magnetic resonance imaging and single-unit intraneural microstimulation. *eLife*, *5*, e12812.

Sanchez Panchuelo, R. M., Schluppeck, D., Harmer, J., Bowtell, R., & Francis, S. (2015). Assessing the spatial precision of SE and GE-BOLD contrast at 7 tesla. *Brain Topography*, *28*(1), 62–65.

Sanchez-Panchuelo, R. M., Besle, J., Beckett, A., Bowtell, R., Schluppeck, D., & Francis, S. (2012). Within-digit functional parcellation of Brodmann areas of the human primary somatosensory cortex using functional magnetic resonance imaging at 7 tesla. *The Journal of Neuroscience*, *32*(45), 15815–15822.

Sanchez-Panchuelo, R. M., Besle, J., Mougin, O., Gowland, P., Bowtell, R., Schluppeck, D., & Francis, S. (2014). Regional structural differences across functionally parcellated Brodmann areas of human primary somatosensory cortex. *NeuroImage*, *93*(Pt 2), 221–230.

Schira, M. M., Tyler, C. W., Breakspear, M., & Spehar, B. (2009). The foveal confluence in human visual cortex. *The Journal of Neuroscience*, *29*(28), 9050–9058.

Schluppeck, D., Sanchez-Panchuelo, R. M., & Francis, S. T. (2017). Exploring structure and function of sensory cortex with 7T MRI. *NeuroImage*, *164*, 10–17.

Schwarz, G. (1978). Estimating the dimension of a model. *The Annals of Statistics*, *6*(2), 461–464.

Sokoliuk, R., Mayhew, S. D., Aquino, K., Wilson, R., Brookes, M. J., Francis, S. T., ... Mullinger, K. J. (2018). Two spatially distinct posterior alpha sources fulfill different functional roles in attention. *bioRxiv*, 384065.

Stelzer, J., Lohmann, G., Mueller, K., Buschmann, T., & Turner, R. (2014). Deficient approaches to human neuroimaging. *Frontiers in Human Neuroscience*, *8*, 462.

Tardif, C. L., Schafer, A., Waehnert, M., Dinse, J., Turner, R., & Bazin, P. L. (2015). Multi-contrast multi-scale surface registration for improved alignment of cortical areas. *NeuroImage*, *111*, 107–122.

Torrisi, S., Chen, G., Glen, D., Bandettini, P. A., Baker, C. I., Reynolds, R., ... Grillon, C. (2018). Statistical power comparisons at 3T and 7T with a GO/NOGO task. *NeuroImage*, *175*, 100–110.

Triantafyllou, C., Hoge, R., Krueger, G., Wiggins, C., Potthast, A., Wiggins, G., & Wald, L. (2005). Comparison of physiological noise at 1.5 T, 3 T and 7 T and optimization of fMRI acquisition parameters. *NeuroImage*, *26*(1), 243–250.

Triantafyllou, C., Hoge, R. D., & Wald, L. L. (2006). Effect of spatial smoothing on physiological noise in high-resolution fMRI. *NeuroImage*, *32*(2), 551–557.

Triarhou, L. C. (2007). The economo-koskinas atlas revisited: Cytoarchitectonics and functional context. *Stereotactic and Functional Neurosurgery*, *85*(5), 195–203.

Turner, R. (2016). Uses, misuses, new uses and fundamental limitations of magnetic resonance imaging in cognitive science. *Philosophical Transactions of the Royal Society B: Biological Sciences*, *371*(1705), 20150349.

Turner, R., & Geyer, S. (2014). Comparing like with like: The power of knowing where you are. *Brain Connectivity*, *4*(7), 547–557.

Uludag, K., & Blinder, P. (2017). Linking brain vascular physiology to hemodynamic response in ultra-high field MRI. *NeuroImage*, *168*, 279–285.

Vaughan, J. T., Garwood, M., Collins, C. M., Liu, W., DelaBarre, L., Adriany, G., ... Ugurbil, K. (2001). 7T vs. 4T: RF power, homogeneity, and signal-to-noise comparison in head images. *Magnetic Resonance in Medicine*, *46*(1), 24–30.

Visser, E., Poser, B. A., Barth, M., & Zwiers, M. P. (2012). Reference-free unwarping of EPI data using dynamic off-resonance correction with multiecho acquisition (DOCMA). *Magnetic Resonance in Medicine*, *68*(4), 1247–1254.

von Economo, C., & Koskinas, G. N. (1925). *Area parietalis (temporo-occipital) basalis*. Wein: Springer.

Vu, A. T., Phillips, J. S., Kay, K., Phillips, M. E., Johnson, M. R., Shinkareva, S. V., ... Yacoub, E. (2016). Using precise word timing information improves decoding accuracy in a multiband-accelerated multimodal reading experiment. *Cognitive Neuropsychology*, *33*(3–4), 265–275.

Worden, M. S., Foxe, J. J., Wang, N., & Simpson, G. V. (2000). Anticipatory biasing of visuospatial attention indexed by retinotopically specific alpha-band electroencephalography increases over occipital cortex. *Journal of Neuroscience*, *20*(6), RC63.

Worsley, K. J., & Friston, K. J. (1995). Analysis of Fmri time-series revisited - again. *NeuroImage*, *2*(3), 173–181.

Worsley, K. J., Marrett, S., Neelin, P., Vandal, A. C., Friston, K. J., & Evans, A. C. (1996). A unified statistical approach for determining significant signals in images of cerebral activation. *Human Brain Mapping*, *4*(1), 58–73.

Wu, J., Ngo, G. H., Greve, D., Li, J., He, T., Fischl, B., ... Yeo, B. T. (2018). Accurate nonlinear mapping between MNI volumetric and FreeSurfer surface coordinate systems. *Human Brain Mapping*, *39*, 3793–3808.

Wu, Q., Li, C. L., Li, Y. J., Sun, H. Z., Guo, Q. Y., & Wu, J. L. (2014). SII and the fronto-parietal areas are involved in visually cued tactile top-down spatial attention: A functional MRI study. *Neuroreport*, *25*(6), 415–421.

Xu, J., Potenza, M. N., & Calhoun, V. D. (2013). Spatial ICA reveals functional activity hidden from traditional fMRI GLM-based analyses. *Frontiers in Neuroscience*, *7*, 154.

Yacoub, E., Shmuel, A., Logothetis, N., & Ugurbil, K. (2007). Robust detection of ocular dominance columns in humans using Hahn spin Echo BOLD functional MRI at 7 tesla. *NeuroImage*, *37*(4), 1161–1177.

Zimmermann, J., Goebel, R., De Martino, F., van de Moortele, P. F., Feinberg, D., Adriany, G., ... Yacoub, E. (2011). Mapping the Organization of Axis of motion selective features in human area MT using high-field fMRI. *PLoS One*, *6*(12), e28716.

Zumer, J. M., Scheeringa, R., Schoffelen, J. M., Norris, D. G., & Jensen, O. (2014). Occipital alpha activity during stimulus processing gates the information flow to object-selective cortex. *PLoS Biology*, *12*(10), e1001965.

SUPPORTING INFORMATION

Additional supporting information may be found online in the Supporting Information section at the end of the article.